CHALMERS
UNIVERSITY OF TECHNOLOGY

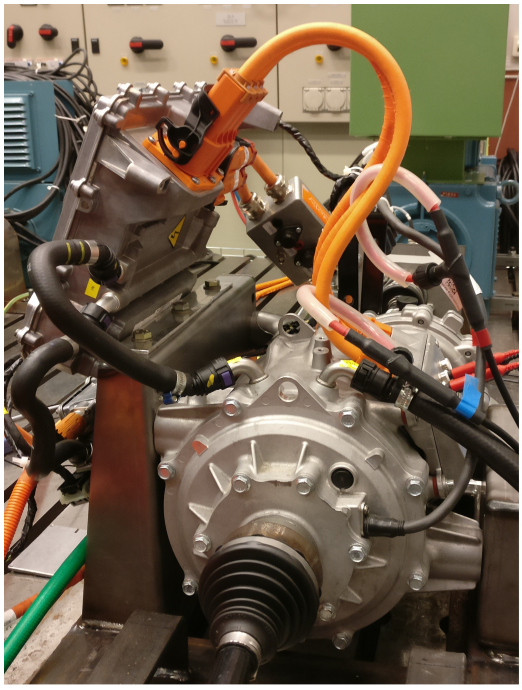

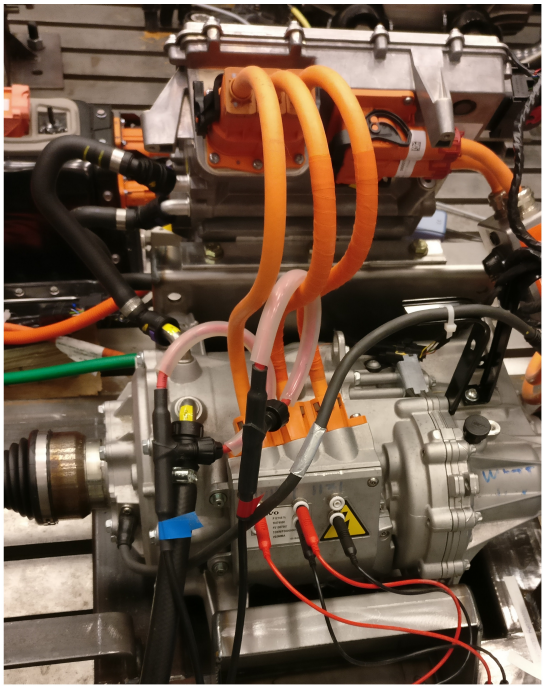

High Power Cables in Electric Vehicles

Analysis of Optimization of High Power Cables Design for both DC and AC in Electric Vehicles

Master's thesis in Electric Power Engineering

Daniel Fahlgren Daniel Heinerås

Department of Electric Power Engineering
CHALMERS UNIVERSITY OF TECHNOLOGY
Gothenburg, Sweden 2017

Master's thesis 2017:05

High Power Cables in Electric Vehicles

Analysis of Optimization of High Power Cables Design for both DC and AC in Electric Vehicles

Daniel Fahlgren Daniel Heinerås

CHALMERS
UNIVERSITY OF TECHNOLOGY

Department of Electric Power Engineering
RIFEL
Chalmers University of Technology
Gothenburg, Sweden 2017

High Power Cables in Electric Vehicles
Analysis of Optimization of High Power Cables Design for both DC and AC in Electric Vehicles
Daniel Fahlgren Daniel Heinerås

Supervisor: Peter Ankarson Henrik Toss Urban Lundgren, RISE
Examiner: Tarik Abdulahovic, Department of Electric Power Engineering

Master's Thesis 2017:05
Department of Electric Power Engineering
Division of Division name
RIFEL
Chalmers University of Technology
SE-412 96 Gothenburg
Telephone +46 31 772 1000

Cover: Test setup for the Volvo XC90 electric powertrain.

Typeset in LaTeX
Gothenburg, Sweden 2017

Abstract

As the demand for cleaner transportation increases around the world, passenger vehicle manufacturers are introducing electric and hybrid powertrains. However, the electric and hybrid powertrains have new issues to deal with, such as electromagnetic interference (EMI) and current ripple generated by the electric drive. To address these issues the manufacturer Volvo has started the Ripple and Electromagnetic Fields in Electric Vehicles (RIFEL) project. This thesis is a part of the project and will focus on the power cables in the Volvo XC90 plug-in hybrid.

There are several methods to reduce the magnetic fields emitted by the cables, including changing the cable arrangement, shielding the cables and twisting the cables. To study and compare these methods, simulations in Comsol and a variety of measurements have been conducted. The results shows that there is a variety of possible solutions to reduce the fields depending on what frequency range the interference occurs at. For high frequencies, shielding with a highly conductive material is a very effective method as long as the shield is properly connected. However, for low frequencies a highly conductive shield has little to no affect. Here the magnetic permeability of the shield is the determining factor of the shield effectiveness. By using a high permeability material with a high conductive material as shield, the magnetic field can be reduced by 19.23 dB at 10 kHz compared to the cable currently in use. Furthermore, the results also shows that by changing the cable arrangement or twisting the cables the magnetic fields can be reduced over the full frequency spectrum from 1 Hz to 10 MHz.

The work also includes modeling of the shielded cable and determination of the cable parameters. To determine the parameters simulations in Comsol and measurements on the cable was used. The results from the measurement shows that the inductance of the cable is 246 nH/m when the shield is not grounded and 94.3 nH/m when the shield is grounded. Furthermore, the simulations shows that the inductance changes with frequency when the shield is grounded. Therefore the model of the cable was made so that these effects could be accounted for.

Keywords: Electric Powertrain, Volvo, Mumetal, Power Cables, EMC, Coroplast, Crosstalk, Shielding.

Acknowledgements

We would like to thank Peter Ankarson, Henrik Toss and Urban Lundgren at RISE for helping us with the report and for letting us use their equipment for important measurements. We would also like to thank Coroplast for being cooperative and providing us with cables for the measurements.

Daniel Fahlgren Daniel Heinerås, Gothenburg, Month Year

Contents

List of Figures

List of Tables

1
Introduction

Tough regulations for emissions from passenger vehicles is putting pressure on the passenger vehicle manufactures to constantly increase power efficiency and reduce emissions. This is one reason many manufactures are looking to replace the conventional internal combustion engine (ICE) powertrain. Volvo is one among many manufacturers who are producing and developing hybrid and electric vehicles as an alternative to the conventional ICE. However, with the hybrid and electric powertrains comes issues not present in the conventional ICE powertrain.

1.1 Regulations for Passenger Vehicles

The number of passenger cars has grown to over one billion worldwide and is expected to keep increasing [3]. Today transportation is responsible for about one fourth of the total energy-related greenhouse gases emitted [3]. To address this issue regulations has been adopted by the European Commission (EU), the United States, Japan and China among others.

One example of regulation to reduce CO_2 emissions is for cars sold in the EU. Here mandatory emission reduction targets has been set for 2021[4]. The target is to reduce the emission from new cars to an average of 95 gram CO_2 per kilometer from 2021 and forward [4]. This can be compared to the 2015's target which was 130 gram CO_2 per kilometer [4]. The target of 95 gram CO_2 per kilometer corresponds to an average fuel consumption of around 4.1 l/100 km of petrol or 3.6 l/100 km of diesel.

In China the average fuel consumption of the total passenger vehicle fleet was 6.9 l/100 km in 2015 according to International Council on Clean Transportation [5]. In 2014 The Chinese Ministry of Industry and Information Technology proposed new restrictions for fuel consumption for passenger cars for 2020. With these restrictions, called phase 4 standards, China aims to increase fuel efficiency to an average of 5.0 l/100 km [5].

Furthermore, besides regulations for fuel consumption and CO_2 emissions, there is restrictions for other particle emissions such as hydrocarbons, carbon monoxides, sulfur oxides and nitrogen oxides. There are different standard levels for these emissions, set for different driving cycles, where the driving cycle used varies depending on the country. A summation of this can be found in Delphi's document, Worldwide Emissions Standards [6], where the emission standards and requirements for specific regions, driving cycles and vehicle types can be found.

1.2 Hybrid and Electric Powertrains

The conventional powertrain with a single internal combustion engine is a refined technology. With tougher regulations, the fuel and emission requirements are reaching the point where the levels are hard to fullfill with a fleet of vehicles using only the conventional ICE powertrain, at the same time as keeping the output power of the engine high enough to satisfy the customers. Therefore, with the increasing requirements on emission levels, manufacturers are producing or looking to produce more vehicles with a hybrid or electric powertrain.

The hybrid vehicle can be classified as a certain hybrid type depending on the electrical capability of the vehicle. The hybrid with the least electrical capability is called micro-hybrid. Here the electric motor only helps to start the ICE and generate power while braking. The mild hybrid can in addition to the micro-hybrid, assist in propelling the vehicle with the electric motor. The full hybrid can fully propel the vehicle with the electric motor and is called plug-in hybrid if it also has the availability to charge the batteries from the electric grid. The electric part of the powertrain in hybrid vehicles often consist of a battery connected to an rectifier and inverter which drives the AC electric machine (EM) as can be seen in 1.1.

Figure 1.1: The electric powertrain with a battery rectifier/inverter and an EM.

1.3 Electric Drive Issues

Inverter manufacturers are striving to minimize size and increase efficiency for their products [7]. This is done through increased switching frequency and therefore shorter rise and fall times. This in combination with the use of pulse width modulation (PWM) techniques results in issues when it comes to integration of the electric drive into the power system. Among the issues are harmonics, high peak currents, excessive dv/dt, additional losses due to eddy currents in the EM, acoustic noise, capacitor stress and poor power quality [7]. This may result in electromagnetic interference and shortened lifetime of the EM [8].

1.3.1 Addition Stress on the Electric Machine

When the supply power from the inverter to the EM is not ideal it will receive additional stress. One of the issues are excessive dv/dt caused by short rise and fall times. High dv/dt on the parallel wires with capacitive coupling in the machine windings cause pole reversal losses. In case of impurities in the insulation hot spots may appear and thus cause damage to the machine. This can especially be a problem for inverters and electric machines connected through short cables where the low inductance allows for the rapid change in voltage to act fully on the windings [7].

Another problem caused by the inverter is voltage overshoots at the EM terminal. Voltage overshoots occurs at higher frequencies when the machine windings appears as capacitive rather than inductive. The capacitance of the EM together with the inductance of the cable then acts as a resonant circuit and thus amplifying the voltage at the machine terminal. This effect will be more substantial for longer cables with higher inductance [7].

1.3.2 Electromagnetic Interference

When electric energy is transferred, electromagnetic fields are induced around the electric link connecting load and source. Whenever the electromagnetic fields are unintended it is classified as electromagnetic noise and when the noise causes interference with other electronics it then becomes electromagnetic interference (EMI) [7]. Electromagnetic noise is generally considered in the range of 0-400 GHz.

In the electric vehicle the electric links operates at 0 Hz at the DC link and 0 to 800 Hz at AC link. However the inverter is operating at higher frequencies and chopping the current which cause high order harmonics which also propagates in the links. Therefore a much higher frequency span than 0 to 800 Hz needs to be considered [9]. The electromagnetic fields can be radiated to the surrounding environment where it can disturb close by electrical systems and cause malfunctions or deteriorate the system [9]. Therefore EMI needs to be taken in consideration to assure safe and reliable systems for hybrid and electric vehicles [9].

The noise can be divided into two types, differential mode noise and common mode noise. In differential mode the conducted signal travels in the phase and back through any of the other phases or through the neutral. This occurs most often at lower frequency often due to inverter switching [7]. The common mode noise unlike the differential mode noise travels in all lines in the same direction. The return path of the signal is through coupling to surrounding electrical return paths. Common mode noise is more likely to occur at higher frequencies.

Coupling in an electrical system can occur in three different ways. It can be galvanic that is to say via electrical contact. The coupling can also be capacitive which will occur when parts in the system are placed close together. A potential difference is required between the objects to create a electrical field and create capacitive coupling. Lastly it can be inductive which requires a current flow that creates a surrounding magnetic field.

To counteract the EMI noise different approaches can be used. One approach is to improve the inverter filters to reduce the noise. Some special filter designs are proposed to address this issue [10], [11]. However one problem with the use of filters is that new noise can be emitted from the filter components. Another approach is to reduce the noise emitted from the transmission links to the surroundings. Here shielding and various configurations of the conductors can be considered to reduce the EMI, more will be discussed in section 2.3.

1.3.3 Non-Ionizing Radiation Health Risks

Besides disturbing electrical equipment, electromagnetic fields can be a risk to human health. This is another concern to manufactures and to people who use vehicles propelled by electric motors. The International Commission on Non-Ionizing Radiation Protection (ICNIRP) is an independent organisation working with health and environmental risks related to non-ionizing radiation i.e. electromagnetic fields at low frequency. They provide scientific advice and guidance for radiation exposure levels. In their report ICNIRP Guidelines for Limiting Exposure to Time-Varying Electric and Magnetic Fields (1 Hz to 100 kHz) they provide guidelines for general public exposure [1]. Their guidelines are based on research conducted by the International Agency for Research on Cancer (IARC), the World Health Organization (WHO) and national expert groups on the biological effects of low frequency electromagnetic fields [1].

A considerable amount of research about cancer related to long term exposure of electromagnetic fields mainly in the frequency range of 50 to 60 Hz has been conducted. In general, no relation were observed. However when it comes to childhood leukemia a small increase was observed for children exposed to higher levels of electromagnetic fields. Whether actually the low frequency electromagnetic fields was the cause or other factors affected the results such as combination of selection bias is uncertain, according to WHOs report Environmental Health Criteria 238 Extremely Low Frequency Fields [12].

For electromagnetic fields ranging from 1 Hz to 10 MHz, ICNIRP came up with reference levels for the general public exposure which can be seen in Table 1.1 where f is the frequency in Hz.

Table 1.1: ICNIRP reference levels for general public exposure of electromagnetic fields from 1 to 10 MHz [1].

Frequency range	Magnetic field H (Am^{-1})	Magnetic flux density B(T)
1 Hz -8 Hz	$3.2 \cdot 10^4/f^2$	$4 \cdot 10^{-2}/f^2$
8 Hz -25 Hz	$4 \cdot 10^3/f$	$5 \cdot 10^{-3}/f$
25 Hz -400 Hz	$1.6 \cdot 10^2$	$2 \cdot 10^{-4}$
400 Hz -3 kHz	$6.4 \cdot 10^4/f$	$8 \cdot 10^{-2}/f$
3 kHz -10 MHz	21	$2.7 \cdot 10^{-5}$

1.4 The RIFEL Project

To increase the level of fuel efficiency, car manufacturers are working on replacing the conventional ICE powertrain with electric or hybrid powertrains. One of the manufacturers producing hybrid cars is Volvo, where one of their plug-in hybrids is the XC90 Twin Engine T8. In the hybrid powertrain the electric engine is connected through a AC-link to the inverter which is feed through a DC-link by the battery.

A Volvo project in collaboration with RISE Research Institutes of Sweden and Chalmers University of Technology has been addressed to overlook the electric powertrain in the XC90 plug-in hybrid. The project is called RIFEL and is supported

by VINNOVA (The Swedish Governmental Agency for Innovation Systems). This report is a part of the RIFEL project and will cover issues related to the AC- and DC-link in the electric powertrain.

1.5 Aim

The aim of this project is to design, compare and evaluate different designs of high power cables for the DC and AC link for the Volvo XC90 hybrid vehicle.

1.6 Technical Targets

Two main areas about the high power cables will be in focus. The main areas are cable parameters and electromagnetic fields. To find and evaluate the most favorable cable it is important to identify what the most favorable parameters and field distributions are for the specific vehicle powertrain application.

The parameters of interest in the cable are resistance, inductance and capacitance between inner conductor and screen, and the screen to the surrounding environment. The resistance is favorable to keep low to reduce losses within the cable. Identifying the most favorable inductance is more complex because it is a trade off between high dv/dt and overvoltages at the EM terminal. Low inductance result in higher dv/dt and high inductance result in higher overvoltages [7].

When it comes to capacitive coupling, it is important to separate between the coupling between the inner conductor to the screen and the coupling in between the inner conductors. The coupling to the screen will result in higher common mode currents which is very likely unfavorable. The coupling between the phase conductor however can be favorable. This because it will act as a filter and thus reducing the harmonics.

Electromagnetic fields are of interest to keep low to assure that the safety levels of non-ionizing radiation for passengers within the car are not exceeded. Low levels of electromagnetic fields also reduce the risk of faulty signals in signal cables and electronics due to EMI.

1.7 Scope

The focus of the project will be on the cables only and the connectors in the ends of the cables will not be included, since this is a separate project by its own. Also the material of the conductor will not be evaluated, since doing research and doing tests for this will be very time consuming and time is a limiting factor for this project.

In this project full focus will be on the cable configurations and the cable shield. Analysis of the insulating materials and aging will not be included due to lack of knowledge in this field. It is important to still acknowledge that this is an important topic due to rough environmental conditions for the cables in the car. Additional strains experienced by the cables may include vibrations, high temperature variations, propagating harmonics and a damp and rough environment.

A more general approach is used in this project which means that more conceptual methods on how to affect the electromagnetic fields will be analyzed. This entails that mainly standardized simulations and measurements will be preformed rather than only focusing on only the specific application.

1.8 Method

In this project, to find the cable parameters and the surrounding electromagnetic fields, both simulations and measurements are used in combination. The reason for this is to validate the results from the simulations by conducting measurements. This could also be used the opposite way around, where the behaviours measured could be explained with phenomenas seen in the simulations. With the simulations it is also possible to test many types of geometries and shielding without actually building them.

The programs used for the finite element simulations are Comsol and FD2D. FD2D is a simple and more easy to understand program. The drawback is that it can only work in 2D and it is not always reliable when it comes to more advanced cable geometries. While Comsol can work with both 2D and 3D geometries and is a more advanced tool. To simulate models of the cables and test setups LTspice was used.

Simple geometries and setups was used at first to reduce errors and easier identify various type of behaviours. Then more complex geometries, similar to the cables in the XC90 was used. If a certain behaviour was unexpected, further simulations or measurements was conducted to understand the cause of it. By following this method it was possible to find explanations for most of the behaviours observed in the results.

The surrounding fields was determined using Comsol simulations and measurements by a network analyser through crosstalk measurements. It is of interest to find the configuration of cables that mitigates the magnetic fields the most. Therefore to compare the performance of different configurations, the electromagnetic field was computed at a determined distance from the cable configurations. The same was done for different types of shielding configurations and shielding materials. This way, by keeping the parameters such as the measuring point, the current applied and others the same, the different cable configurations could be compared to each other.

2

Electrostatic and Electromagnetic Field Theory

This chapter contains the underlying theoretical concepts involved in this study. This is to get an understanding of the physics and science behind the electric and electromagnetic phenomenas acting within and around the cables in the hybrid powertrain.

2.1 Electrostatics and Electric Currents

As mentioned in the introduction, two central concepts in this study are common mode and differential mode currents. CM currents are the current flowing from the inner conductor to the shield and DM current is the current into one of the inner conductors and back through another inner conductor. The CM and DM currents are affected by the cable properties which determines the resistive, capacitive and inductive coupling in between the inner conductor and the screen, while also between the inner conductor and the surrounding [9].

In this study the cable resistance will be calculated by hand and the other parameters, capacitance and inductance will be calculated mainly numerically using finite element solvers. In the case of capacitance, both capacitive coupling between the conductor and screen as well as capacitive coupling between the screen and the ground plane will be examined. The resistance R for a cable and DC current can be calculated as

$$R = \frac{l \cdot \rho}{A} \tag{2.1}$$

, where l is the length of the cable, ρ is the resistivity of the conductor and A is the cross-section area of the conductor. When AC current propagates in conductors a current in the opposite direction is induced in the center of the conductor. This so called skin effect therefore reduces the current flowing in the center of the conductor. A parameter related to the skin effect is the skin depth δ. The skin depth is the penetration depth seen from the surface where current flows and inwards. The skin depth can be calculated as [13]

$$\delta = \sqrt{\frac{2\rho}{w\mu}} \tag{2.2}$$

, where μ is the permeability, w is the angle velocity of the current and ρ is the

resistivity of the conductor. For a known skin depth the resistance can be calculated as for a round conductor

$$R = \frac{l\rho}{A - \pi(r-\delta)^2} \tag{2.3}$$

, where r is the radius of the conductor. This is a modification of (2.1), with the area A restricted by the skin depth. This expression is valid only for $r >= \delta$ since the skin depth cannot be greater than the radius of the conductor. For higher frequencies (2.3) can be simplified to [13]

$$R = \frac{l\rho}{2\pi r\delta}. \tag{2.4}$$

To find the capacitance two different methods are used in this study. The first method is based on the charge on the conductor and voltage potential relation. Here the capacitance of a cable can be defined as

$$C = \frac{Q}{V}. \tag{2.5}$$

In this method, an expression for the charge Q per unit length is required. This can be derived from Gauss-Maxwell's equation for electric fields

$$\nabla(\varepsilon_0\varepsilon_r E) = p_v \tag{2.6}$$

, where ε_0 is the permittivity of vacuum, ε_r is the relative permittivity of the material, p_v and E is the electric field. The Gauss equation can be rewritten to integral form as [14]

$$\frac{Q}{\varepsilon_0} = \oint_{\partial S} \vec{E} \bullet \hat{n}, dS. \tag{2.7}$$

In (2.7) S is the surface which encloses the total charge Q inside and $\hat{n}$ is the direction out of the surface S. The electric field E can be written as (2.8), where V is the potential.

$$E = -\nabla V. \tag{2.8}$$

To find ∇V, (2.8) is inserted to (2.6) and the whole domain is considered including grounded conductors or grounded planes where negative charge is accumulated. This entails that the sum of the total charge enclosed is equal to zero and therefore the expression in (2.9) can be derived.

$$\nabla(\varepsilon_0\varepsilon_r\nabla V) = \varepsilon_0\varepsilon_r(\frac{\partial^2 V}{\partial x^2} + \frac{\partial^2 V}{\partial y^2}) = 0. \tag{2.9}$$

In (2.9) only the two dimensional space is considered which will work for long straight cables where the potential difference in $\hat{z}$ can be approximated to zero. Solving (2.9) can be done numerically using finite element solvers. To get the capacitance per unit length, (2.7) can be solved for a line on the surface of the conductor in the xy-plane instead of an area for long straight cables.

The second method that is used is based on the total electrostatic energy stored W_e. The total electrostatic energy can be derived through volume integration of the whole insulating domain between the conductor and the grounded conductor or grounded plane. The capacitance can then be found using (2.10) if the voltage V applied on the conductor is known.

$$W_e = \frac{CV^2}{2}. \tag{2.10}$$

In this study, it is of interest to find not only the total capacitance but also the capacitance's between a set of conductors so that a more accurate circuit model can be used. To find the interpolated capacitance's between objects a Maxwell capacitance matrix is introduced. The matrix can be calculated by preforming a series of calculations or measurements, where potential and ground is assigned to the objects in a series of different ways.

In the case of conductors above a ground plane with no magnetic materials present, the inductance matrix can be found from (2.11) [15], for a known capacitance matrix.

$$L = \varepsilon_0 \mu_0 C_0^{-1}. \tag{2.11}$$

In (2.11) L is the inductance matrix, μ_0 is the relative permeability and C_0 is the capacitance matrix. Another way of calculating the inductance per unit length is through surface integration of the magnetic energy W_m as

$$\frac{2}{I} \iint_V W_m dxdy = L \tag{2.12}$$

where I is the current in $\hat{z}$ direction.

2.1.1 Capacitance between Inner Conductor and Shield

For simple geometries it is possible to calculate the capacitance by hand. One simple and relevant geometry is a long round conductor surrounded by a larger cylinder representing a shielded cable as illustrated in Figure 2.1 where r_1 is the radius of the inner conductor and r_2 is the radius of the insulation.

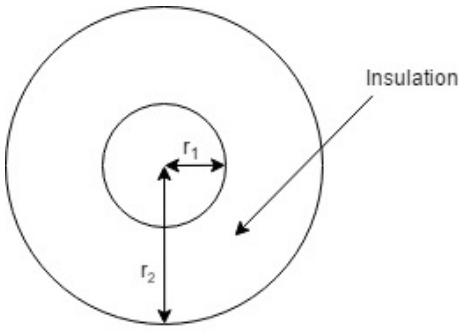

Figure 2.1: Cross section of a shielded cable.

To find the capacitance an expression of the electric field in between the inner conductor and screen is derived using (2.7) with the surrounding area which is equal to the circumference times the length i.e. $2\pi l$.

$$E = \frac{q}{2\pi r \varepsilon_0 l} \tag{2.13}$$

Now an expression for the voltage potential can be derived from combining (2.8) with the new expression of the electric field (2.13) to

$$V = \frac{q}{2\pi\varepsilon_0}\int_{r_2}^{r_1}\frac{1}{r}dr = \frac{q \cdot ln(\frac{r_1}{r_2})}{2\pi\varepsilon_0 l}. \tag{2.14}$$

Finally, insertion of (2.14) into (2.5) gives an expression of the capacitance dependant of the geometry parameters

$$C = \frac{2\pi\varepsilon_0 l}{ln(\frac{r_2}{r_1})}. \tag{2.15}$$

2.1.2 Capacitance between two Parallel Conductors

Another simple and interesting geometry is two parallel conductors in free space as illustrated in Figure 2.2 where r is the radius of the conductor and D is the center to center distance between the two conductors.

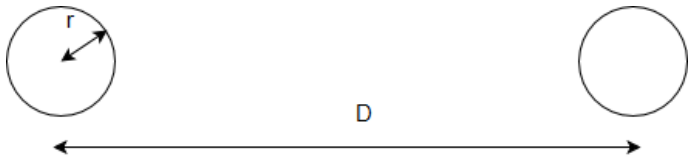

Figure 2.2: Two parallel wires conductors in free space.

A similar approach as used in section 2.1.1 can be used to find the capacitance for this geometry. This is done by imagining only one of the conductors in free space. The potential difference to a point of distance D from the conductor center is then

$$V = \frac{q}{2\pi\varepsilon_0}\int_{D}^{r_c}\frac{1}{r}dr = \frac{q \cdot ln(\frac{r_c}{D})}{2\pi\varepsilon_0 l}. \tag{2.16}$$

Now if both conductors has the same radius and the other conductor has the same charge but negative its contribution to the potential difference will be of the same magnitude. Now insertion of (2.16) times two into (2.5) gives

$$C = \frac{\pi\varepsilon_0 l}{ln(\frac{D}{r_c})}. \tag{2.17}$$

However this is only true for geometries where $D >> r$ [16].

2.1.3 Resonant Circuit

A resonant circuit is a circuit with a inductor and a capacitor either placed in series or parallel. Figure 2.3 displays an illustration of the undamped series resonant circuit.

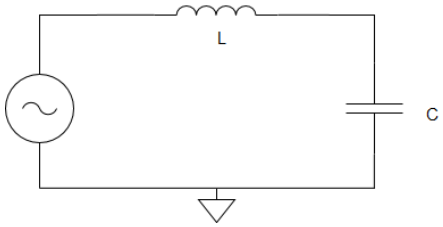

Figure 2.3: Undamped series resonant circuit.

The resonant circuit will at a certain frequency reach a point where the reactance from the inductance and capacitance cancel out each other. This frequency is the circuits resonant frequency F_0. The resonant frequency can be calculated as (2.18) for a series resonant circuit[17].

$$F_0 = \frac{1}{2\pi\sqrt{LC}} \tag{2.18}$$

A resonant circuit can be used to measure the cable parameters. This can be done by creating a resonant circuit with a known capacitance or inductance and the cable and measuring the resonant frequency. This way the cable inductance or capacitance can then be derived from (2.18).

2.2 Electromagnetic Fields

Electromagnetic fields are generated by a flow of electric current. In this study the focus is on how the electromagnetic field and flux is affected by the path the current flows from one point to another. The electromagnetic flux for a specific point in space can be calculated as [14]

$$d\vec{B} = \frac{\mu_0}{4\pi}\frac{\mathbf{I}d\vec{l}\times\vec{r}}{r^2} \tag{2.19}$$

according to Ampere´s law . In (2.19), **I** is the magnitude of the current, r is the distance between the specific point and the position where the current flows and dl is the current path line divided into smaller sections. The direction of the magnetic field is determined by the cross multiplication of the specific direction of the current in one section $\vec{dl}$ and the direction of unit vector from the current element in one section to the specific point of interest. The total magnetic flux in the point can be calculated by summation of the contribution of all current elements as

$$\vec{B} = \sum_{i=1}^{n} d\vec{B_n}. \tag{2.20}$$

Another approach, perhaps more suitable for hand calculations, is to consider another expression of Ampere's law. According to Ampere's law the magnetic field along an enclosing line is proportional to the current which is enclosed as following [8]

$$\oint H\,dl = I \tag{2.21}$$

where l is the enclosing line and H is the magnetic field. When conductors with current traveling in opposite directions the sum of the enclosed current can be close or equal to zero. This entails that the magnetic field around the conductors is reduced [8].

For the same geometry shown in Figure 2.2, consisting of two parallel conductors in free space, it is also interesting to also find the inductance. The inductance can be expressed as

$$L = \frac{\psi_m}{I} \tag{2.22}$$

where ψ_m is the total magnetic flux. According to Ampere's law (2.21) the magnetic field can be expressed as

$$\vec{B} = \frac{\mu_0 I}{2\pi r}\hat{\varphi} \tag{2.23}$$

for a conductor carrying the current I in free space at distance r from the conductor. If the same current is traveling back through the second conductor it is known from Ampere's law (2.21) that the magnetic flux enclosing both conductors is equal to zero since currents cancel out each other. Therefore only the surface in between the conductors needs to be considered and the total magnetic flux can be calculated

$$\psi_m = 2\int \vec{B}d\vec{S} = \frac{2l\mu_0 I}{2\pi}\int_{r_c}^{D-r_c}\frac{1}{r}dr = \frac{2l\mu_0 I}{2\pi}ln(\frac{D-r_c}{r_c}). \tag{2.24}$$

Since both currents induces a magnetic field in the same direction and the magnitude of the field is of the same magnitude a factor two is included in (2.24). Insertion of (2.24) into (2.25) gives an expression of the inductance dependant on the geometry parameters

$$L = \frac{l\mu_0}{\pi}ln(\frac{D-r_c}{r_c}). \tag{2.25}$$

Another way to the determine the inductance which perhaps is more suitable for numerical simulations is from the total magnetic energy W_m stored when a current is propagating in the wire

$$L = \frac{2W_m}{I^2}. \tag{2.26}$$

Here W_m can be found through integrating the entire domain of the wires and surroundings.

2.3 Magnetic Field Radiation Reduction

To reduce the electromagnetic fields radiated around cables a number of different approaches can be used. The approaches that are considered in this study are twisting of the cables, shielding of the cables and rearrangement of the cable configuration.

2.3.1 Twisting the Cables

One of ways to reduce the magnetic field radiation can be to twist the cables so the magnetic field from the conductors cancel out each other in a higher degree. According to the report "Recommendations for Mitigating Low Frequency Magnetic Field Exposure in Hybrid/Electric Vehicles" it should be a efficient method and also from the article "Reduction of Power System Magnetic Field by Configuration Twist" some experiments with a helix configuration was done and proved to reduce magnetic field [18], [19]. In the article a simple equation was presented for calculating the magnetic field reduction, it states

$$F = \sqrt{\frac{\pi}{2}}\gamma^{3/2}e^{-\gamma} \tag{2.27}$$

where F is the field reduction twist factor and

$$\gamma = \frac{2\pi r}{p} \tag{2.28}$$

where r is the distance from the measuring point to the line and p is the pitch angle.

The twist factor can be applied for two and three cables, but only the two cable case will be used in this report in order to only get a understanding on what twisting the cables can do to the magnetic field. According to the article "Reduction of Power System Magnetic Field by Configuration Twist" the magnetic field for the helix conductor is written as

$$B_r = 2\frac{\mu_0 Ia}{\pi r^2}\gamma^2 \sum_n^\infty nI_n'(n\eta)K_n'(n\gamma)sin(n(\theta - kz)) \tag{2.29}$$

$$B_\theta = 2\frac{\mu_0 Ia}{\pi r^2}\gamma \sum_n^\infty nI_n'(n\eta)K_n(n\gamma)cos(n(\theta - kz)) \tag{2.30}$$

$$B_z = -2\frac{\mu_0 Ia}{\pi r^2}\gamma^2 \sum_n^\infty nI_n'(n\eta)K_n(n\gamma)cos(n(\theta - kz)) \tag{2.31}$$

where $\eta = \frac{2\pi a}{p}$, $k = \frac{2\pi}{p}$, μ_0 is the magnetic permeability of free space, I is the applied current, a is the radius distance from the center out to the two conductors, $I_n(z)$ and $K_n(z)$ are Bessel functions of first and second order n. The derivative of the functions are $I_n'(z)$ and $K_n'(z)$. In the article an approximation of the Bessel functions was made for the untwisted pair and it follows as

$$I_l'(\eta) \approx \frac{1}{2} \tag{2.32}$$

$$K_l(\gamma) \approx \frac{1}{\gamma} \tag{2.33}$$

$$K_l'(\gamma) \approx -\frac{1}{\gamma^2} \tag{2.34}$$

which gives

$$B_r \approx B_0 sin\theta \tag{2.35}$$

$$B_\theta \approx B_0 cos\theta \tag{2.36}$$

$$B_z \approx 0 \tag{2.37}$$

$$B \approx B_0 \tag{2.38}$$

where $B_0 = \frac{\mu_0 Ia}{\pi r^2}$. The approximation for the twisted pairs states

$$K_l(\gamma) \approx -K_l'(\gamma) \approx \sqrt{\frac{2}{\pi\gamma}e^{-\gamma}} \tag{2.39}$$

and $I_l'(n)$ have same approximation as for the untwisted cables. By combining these with (2.27), the field approximation states for two twisted cables

$$B_r \approx FB_0 sin(\theta - kz) \tag{2.40}$$

$$B_z \approx FB_0 cos(\theta - kz) \tag{2.41}$$

$$B_\theta \approx 0 \tag{2.42}$$

$$B \approx FB_0 \tag{2.43}$$

The effective value of the field for the twisted cables can be approximated to this when $r >> p$ and $a << p$ while in the untwisted case $p >> r$.

2.3.2 Cable Configuration

The arrangement of the cables is one important factor which determines the magnetic fields. For a DC system with one conductor for positive and one for negative potential the separating distance is the main variable. For the three phase system on the other hand the cables can be placed in a line or a delta configuration which would be more symmetrical.

Another way of arranging the cables is to use more than one conductor for each phase. This will allow for new types of arrangements. For example, with the use of four conductors instead of two it is possible to get a more symmetrical system by placing the positive and negative phase conductors in a diagonal square configuration. Similar configurations can also be used for a three phase system where three conductors can be split to six, where one efficient arrangement is to put them in a triangle shape which shows significant reduced magnetic field radiation [18].

2.3.3 Shielding the Cables

The use of a shield around the inner conductor will reduce the electromagnetic fields outside the cable. The shield will work as a blockade between the source of the electromagnetic fields and the areas which needs protection from it. In order to reduce the electromagnetic field emitted by the cables a high conductivity material is preferably used in the shielding, such as copper and aluminium. For a constant plane such as a long straight cable (2.44) can be used to determine the best material for the shield [20].

$$\gamma = \alpha + j\beta = \sqrt{j\omega\mu(\sigma + j\omega\varepsilon)}. \tag{2.44}$$

In (2.44) γ is the propagation constant, α is the attenuation constant β is the phase constant μ, σ and ε is the permeability, conductivity and permittivity respectively. By using high values for μ and σ a high value for α will be achieved and therefore also an increase in the shielding properties of the shield [20], [21]. Shielding effectiveness (SE) is a way to determine the effectiveness of a shield. The total SE can be determine by three equations describing the Absorption loss, Reflection loss and the Re-Reflection correction factor. However the correction factor is considered if the Absorption loss is less then 10 dB. The Absorption loss is the loss absorbed by the shield and is given by

$$A(dB) = 131.4l\sqrt{\mu_r\sigma_r f} \tag{2.45}$$

where A is the absorption loss in dB, l is the thickness of the shield in meters, f is the frequency, μ_r is the relative permeability and σ_r is the electrical conductivity. The Reflection loss for magnetic fields is the loss from the reflections between the shield and the second medium in this case the inner insulation layer. The reflection loss increases when the impedance differs from the shield to the second medium and can be expressed as

$$R_m = 20log\left[\frac{0.0117}{r\sqrt{f\sigma_r/\mu_r}} + 5.35r\sqrt{f\sigma_r/\mu_r} + 0.354\right] \tag{2.46}$$

where r is the distance from the source to the shield. After the reflection loss there can be a re-reflection loss which can be necessary to include. The re-reflection loss can be expressed as

$$C_m = 20log\Big[1 - \gamma(cos0.23A - jsin(0.23A))\Big] \tag{2.47}$$

where γ is

$$\gamma = 4\frac{(1-m^2)^2 - 2m^2 + j2\sqrt{2}m(1-m)^2}{((1+\sqrt{2}m)^2+1)^2} \tag{2.48}$$

and where m is

$$m = \frac{4.7 \cdot 10^{-2}}{r}\sqrt{\frac{\mu_r}{\sigma_r}} \tag{2.49}$$

By summarising (2.45), (2.46) and (2.47) the magnetic shield effectiveness can be calculated [22].

For high frequency electromagnetic fields the absorption and reflection losses are high and the magnetic field can effectively be reduced by using a high conductive material such as copper or aluminium. The material will create a magnetic field that induces eddy currents in the shield which generates a magnetic field in the opposite direction. An increase of frequency of the signal will increase the coupling and therefore increase the induced eddy currents and shield effectiveness [23].

At low frequency the absorption and reflection loss are much lower and the magnetic field is harder to reduce, therefore a high relative permeability material such as steel or mumetal is a better choice. Since it has high permeability the magnetic field will follow a magnetic shunt path in the shield and protect the outside from the magnetic field [24]. For most materials with high relative permeability, the relative permeability is reduced with the increase of frequency [25]. This is especially true for certain types of materials such as mumetal. Therefore materials with high permeability decrease in effectiveness for magnetic fields above 1 kHz.

Since the shield effectiveness is dependent on induced currents, the way the shield is connected can therefore play an important role on its effectiveness. In G.L. Skibinski, R.J. Kerkman and D. Schlegel article EMI emissions of modern PWM AC drives a test with a drive analog interface signal connected to a 2 kΩ load through a 60 meter long twisted and shielded cable [8]. The test was repeated for various shield connections where the ground at the load side is zero potential and the ground at the drive side is connected to the steel structure through a 190 meter cable and the grounding is therefore noisy. The results was that noise voltage was suppressed the most if both ends of the shield was grounded and least if the drive end was connected. Even leaving both ends open gave better suppression than connecting the cable to the noisy drive ground [8].

2.4 Lorentz Force

When electric current flows in a conductor a magnetic field force will act on the conductors. The force acting on a charged particle is described by Lorentz equation which can be expressed as [26]

$$\mathbf{F} = q(\mathbf{E} + \mathbf{V} \times \mathbf{B}) \tag{2.50}$$

where q is the elementary charge and $\mathbf{V}$ is the velocity of the particle. If only the force generated by the magnetic field is considered and the total number of charges in a conductor is considered, the total force per length acting on a conductor can be derived.

$$\frac{\mathbf{F}}{\Delta L} = \mathbf{I} \times \mathbf{B} \tag{2.51}$$

In (2.51) ΔL is the length of the conductor and $\mathbf{I}$ is the current which flows in the conductor. When two conductors are placed in parallel each of the conductors will induce a magnetic field which act on the other when there is a flow of current. For conductors with current in opposite directions the force will be outwards as illustrated in Figure 2.4. For conductors with current in the same direction the force will instead act inwards.

Figure 2.4: Lorentz force acting on two parallel conductors with current in opposite direction.

3

Cable Modeling and Simulations

This chapter will cover the general procedure of how the simulations are conducted. It will also cover how the simulations can be verified by using the parameters derived in a simple two wire model and comparing it to measurement of the same simple setup.

Finite elements solvers are used to calculate the electric and electromagnetic fields generated by the charge and the flow of electric current. The capacitive and inductive couplings can be also be determined from the fields. Finite element solvers can also be used to solve for electromagnetic forces and thermal fields among other things.

3.1 Modelling and Simulating the Magnetic Field for Different Geometries in Comsol

In order to test how good the field cancellation is for various cable arrangement a new simulation has to be preformed for each one of the arrangements. The cables are build in ether a normal 2D geometry or 2D-axisymmetric. All the cables arrangements are placed in the middle of a 500 mm radius circle which is the air domain outside of the cables. When 2D-axisymmetric is used, both the cable and the air domain is placed 20 meters away from the center. This in order simulate the behavior of a straight cable and to get a closed loop for the cables.

When the cable geometries are built, the next step is to define the materials. The materials used in this study are copper, air and silicon rubber. Copper and air are already standard materials in Comsol and the silicon rubber was made using a blank material and assigning it its material properties. Since the goal is to reduce the magnetic field strength outside of the cable, the chosen physic is Magnetic Fields (mf), note that when using Magnetic Fields the only material properties that are necessary are permittivity, permeability and electric conductivity. With Magnetic Fields as physic the domain that represents the conductor is deselected. This since the induced currents in the conductor is not wanted in order to keep the total current in the conductor fixed. The simulations are preformed over a broad frequency spectrum and as mentioned in the theory section 2.1 the current is affected by the skin effect at higher frequencies, therefore when applying current to the conductors Surface Current in (mf) is chosen for each phase. The surface current density is chosen so that the total current over the circumference of the conductor becomes 1 ampere. For the DC case the current is positive in one cable and negative in the other. For AC the current applied is shifted with 120° for each phase, the current is still 1 ampere but multiplied with $\sin(\omega t+\phi)$.

Before the simulation can start a mesh needs to be applied. Since the shield is very thin an accurate mesh on the shield can not be achieved with the normal physics controlled mesh. User controlled is instead chosen and under Boundary Layer Properties the boundaries for shield and conductor are marked. Under Size select, predefined and select extremely fine. As can be seen in Figure 3.1 the mesh is very fine at the conductive boundaries. This is important to accurately simulate the induced currents at higher frequencies.

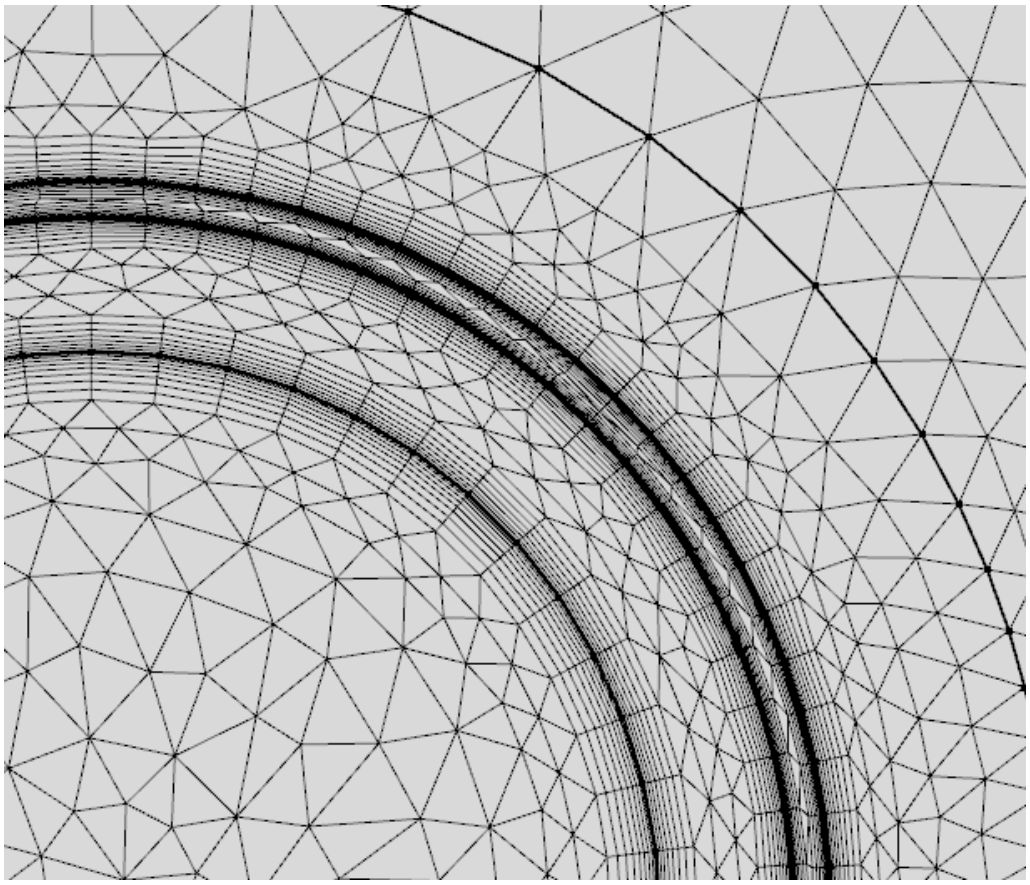

Figure 3.1: The applied mesh for the cable in Comsol.

The final step is to define the study. For the DC arrangements, frequency domain study with the range of 1 Hz to 10 MHz was used. When the simulation is preformed a point in the domain can be selected under Data Sets. A 1D plot group can then be picked and under it the Point Graph option can be used on the point from Data Sets. The results will then show the magnetic flux density at various frequencies in that specific point.

For AC geometries the same study with the same frequency is chosen but under study extensions auxiliary sweep is selected. Here the parameter wt for the current is defined from 0 to 2π. This is done in order to get the magnetic flux density for a full periodic sweep for every frequency. When the simulation is finished, point evaluation can be selected under derived values to get the average field in one point for the full wt sweep. This is done using the average operation. The derived average value of the magnetic flux can then be plotted the same way as for the DC cable

geometries.

3.2 Modelling and Simulating Non-Linear Ferromagnetic Materials in Comsol

For some materials the material properties may vary depending on the frequency. One such non-linear material is mumetal which has a high permeability at low frequencies that decreases for for higher frequencies. To simulate this behaviour in Comsol the material is created as a blank material where the fixed properties are assigned as in section 3.2. However for the non-linear parameters, i.e. the permeability for the mumetal, the parameters is instead assigned by importing the permeability over frequency dependency data for the material. Under the material section in Comsol, a interpolation function can save the data as a function and replace it at relative permeability section. The material will now be able to change its properties with the frequency.

3.3 Choosing the Measuring Point

When measuring the magnetic field the measuring point for each simulation needs to be the same for all tests in order to get to be able to compare the tests. The measurement point is a point 100 mm from the center of the cable bundle where the magnetic flux is the highest. This point can be determined by measuring the magnetic field along a quarter of a circle with radius 100 mm and the center point in the same position as the cable bundles center. In Figure 3.2 a results of such a measurement can be seen. Here the cables were placed next to each other and arc length 0 mm represents straight above and 160 straight to the side of the bundle. Since the point to side of the cables has the highest flux this point was chosen as the measurement point.

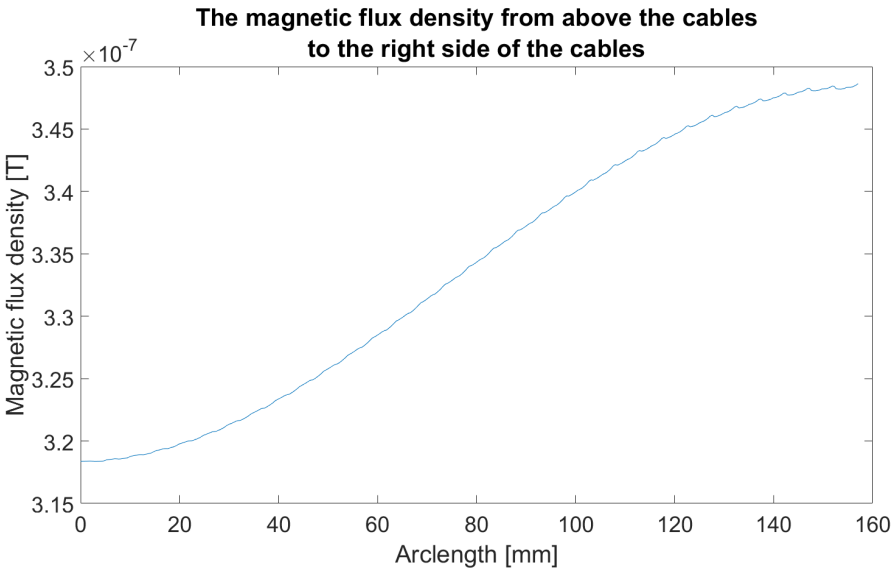

Figure 3.2: The magnetic flux density along a quarter of a circle with radius 100 mm from a point 100 mm above the cables to a point 100 mm to the right of the cable.

3.4 Modelling and Simulating the Cable Temperature Development in Comsol

When simulating the heat dissipation in the cables, most of the steps are the same as in section 3.2. The geometry is the same except that the air domain is removed since the temperature in the air is not of interest. Heat transfer in solids is used and therefore new parameters for the materials is needed such as density, thermal conductivity and heat capacity at constant pressure. The physics used is Heat transfer in solids and the conductor is deselected. This since the temperature in the insulation and shield is the main focus and the temperature in the conductor can be expected to be uniform due to its higher thermal conductivity. The initial temperature is chosen to be 293.15 kelvin, then Heat Flux is selected on the outer boundaries of the insulation. The Heat transfer coefficient is chosen to External natural convection for Long horizontal cylinder with air as the external medium. On the inner boundary between the insulation and the inner conductor a new boundary Heat Flux is created. Here General inward heat flux is selected with the injected power equal to the losses per meter in the cable divided with the circumference of the conductor. The losses per meter can be calculated as the current square times the resistance per meter. For the common shield geometries, Heat transfer in fluids instead of solids is necessary as Physics in order to simulate air inside of the cable. This is done by choosing gas/liquid under thermodynamics and then marking the air domains. Extremely Fine Mesh is used and Time dependent study with a time span of 0 s to 4000 s which is about the time needed to reach steady state. Now the results can be presented in a 1D plot group as before and the chosen measuring point is the warmest point on the conductor boundary.

3.5 Inductance and Capacitance Matrix Simulations for Two Straight Copper Wires

To calculate the inductance and capacitance matrix both FD2D and Comsol is used. In the first simulation the inductance and capacitance between two thin copper wires above a ground plane is examined. The diameter of the wires are 2 mm and they are placed at various distance between each other and at various height above the ground plane as can be seen in 3.3.

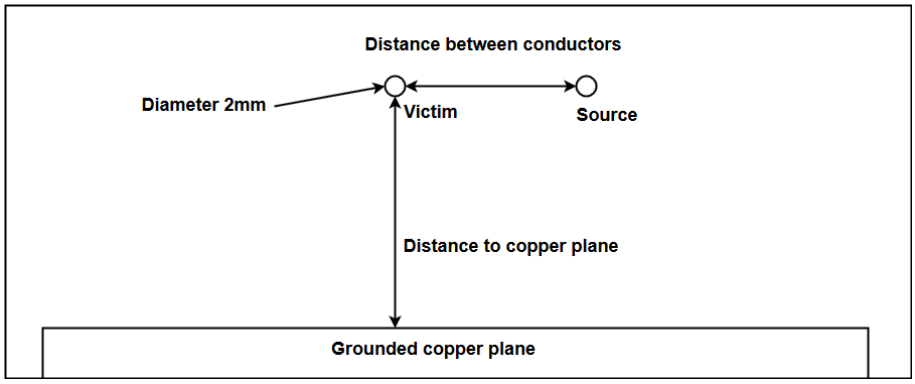

Figure 3.3: The setup with two wires above a ground plane.

In Comsol, 2D geometry is used together with electrostatic physics to calculate the capacitance. The materials used are the built in copper and air. The mesh used is finer physics controlled mesh. The total capacitance is calculated to 9.625 pF/m using (2.5) and to 11.793 pF/m using (2.10). The capacitance matrix is calculated by assigning terminals to each of the conductors and the ground plane. The results can be found in Table 3.1 for various distance between the wires and height above the ground plane.

The same thing can be done in FD2D. In order to calculate the L and C matrix for two standard copper wires the following needs to be done: FD2D does not have any SI units so the scaling is done manually, a grid with 1000 x 700 units is used and one distance between two dots for the grid is corresponding to 0.5 mm. For this the planes around are grounded at 0 potential and the two wires together are placed at two different heights and two different lengths between the each other. When the wires are set the program calculates the inductance of the wires, the mutual inductance, the capacitance between the wires C_{21}/C_{12} and the total capacitance. To calculate C_{23}/C_{31} which is the capacitance from the wire to ground, the total capacitance is taken minus the capacitance between the two wires C_{21}. The derived capacitance's can be seen in Table 3.1.

Table 3.1: Capacitance for two copper wires calculated using Comsol and FD2D

Height above ground plane [mm]	Distance between wires [mm]	Comsol C_{21}/C_{12} [pF/m]	Comsol C_{31}/C_{32} [pF/m]	FD2D C_{21}/C_{12} [pF/m]	FD2D C_{31}/C_{32} [pF/m]
60	30	3.89	8.71	3.66	9.28
60	60	2.17	9.63	1.89	10.40
120	30	4.83	6.72	4.24	8.05

To find the inductance Comsol's Magnetic field physics is used with the same 2D geometry and settings as when calculating the capacitance. The inductance can be found by surface integration of the magnetic energy W_m on the surrounding air as (2.12) shows. In FD2D the calculated mutual inductance is given as a unitless factor which was implemented in to the Pi section in LTspice to simulate the mutual inductance. The inductance is also calculated analytically using the capacitance matrix as in (2.11). The results for the inductance derived using the different methods can be seen in Table 3.2.

Table 3.2: Inductance for two copper wires calculated using Comsol, FD2D and the C_0-matrix.

Height [mm]	Distance [mm]	L/m Comsol [μH/m]	L/m FD2D [μH/m]	L/m from C_0[μH/m]	Mutual inductance factor FD2D	Mutual inductance factor Comsol
60	30	0.956	0.935	0.98	0.281566	0.2948
60	60	0.956	0.926	0.98	0.154366	0.1668
120	30	1.090	1.025	1.17	0.328571	0.3776

From the results it can be noticed that the inductance calculated analytically and with the different finite element solvers does not differ much. Comsol is probably more accurate than FD2D since the geometry and mesh is more uniform.

3.6 Circuit Model in LTspice

To simulate the behaviour of the cable a circuit model is created. The program used for this is LTSpice and the model used for the cables are the pi model. Since wires and cables used in this study are short a series of pi models are not needed [27]. For a simple setup consisting of two parallel copper wires a pi-section in LTspice was build which can be seen in Figure 3.4. With this the gain i.e. V_{out}/V_{in} can be simulated and presented in a graph for a frequency sweep.

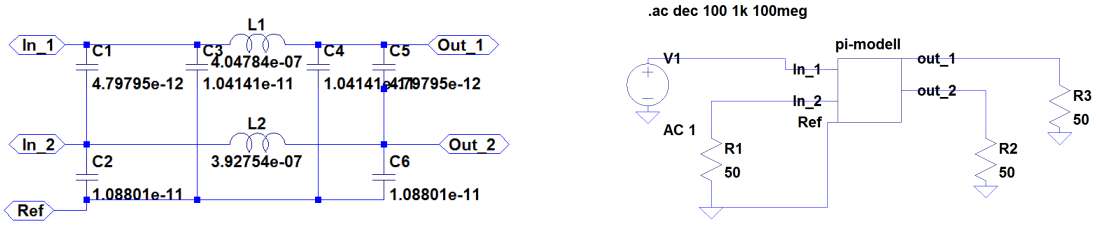

(a) (b)

Figure 3.4: a) The pi model of the two copper wires and b) the measurement setup

The model presented in Figure 3.4a is made for single conductors and does not include cable shields. For shielded cables a more advanced model is needed. Figure 3.5 shows a model which includes the shields where the parameters was found using Comsol. In FD2D the parameters could not be extracted since adding the shield to the simulation gave values which were out of the range of being considered to be correct. As mentioned before FD2D have its limitations when it comes to more complex cable geometries and therefore for further simulations FD2D will not be used. A third victim[1] line can be added to the model to simulate the gain induced when a signal propagates in the cables.

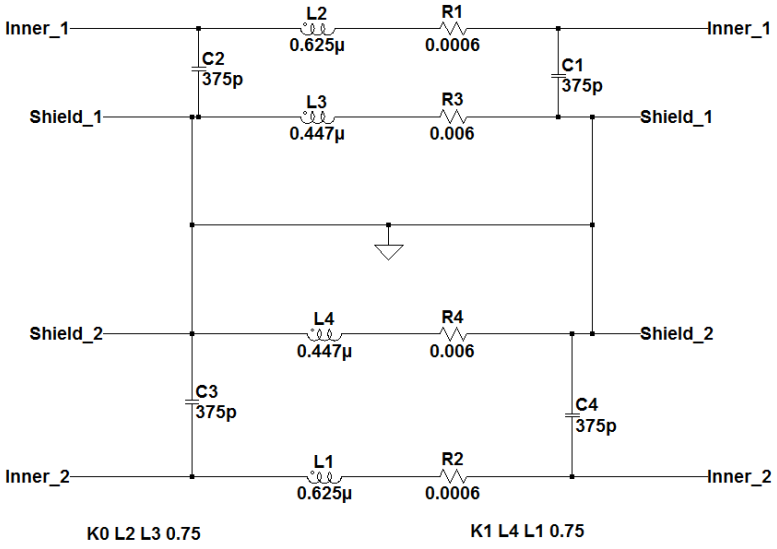

Figure 3.5: The pi model for two cables in.

In Figure 3.5, L1 and L2 are the inductance of the inner conductor and L3 and L4 are the shields inductance. An electromagnetic coupling is added between the inner conductor and shield. The magnetic coupling between shield 1 to inner conductor 2 of the other cable is included in the model in the inner-to-shield coupling factor and the same for shield 2 and conductor 1. The way this works is because it is the same current that flows in the second cables inner conductor but in the opposite direction which therefore can be included by a slight reduction in the inner-to-shield coupling factor.

[1] A wire where the level of EMI emitted by the system is measured.

When it comes to capacitance, the only capacitance included in the model is the capacitance between the inner conductor and the shield. Capacitance in between the shields and between the shields and ground are neglected in this model. This is because these capacitance's will not have a significant affect on the impedance of the cable at low frequency. The parameters in the circuit model can be changed to more extreme values to get a better understanding of their effect on the impedance of the model. By increasing the coupling factor and shield resistance and reducing the cable resistance and simulating the differential mode impedance, the impedance in Figure 3.6 can be derived. In this simulation a voltage source is applied on the inner conductors in one of the ends and the inner conductors are short circuited in the other end.

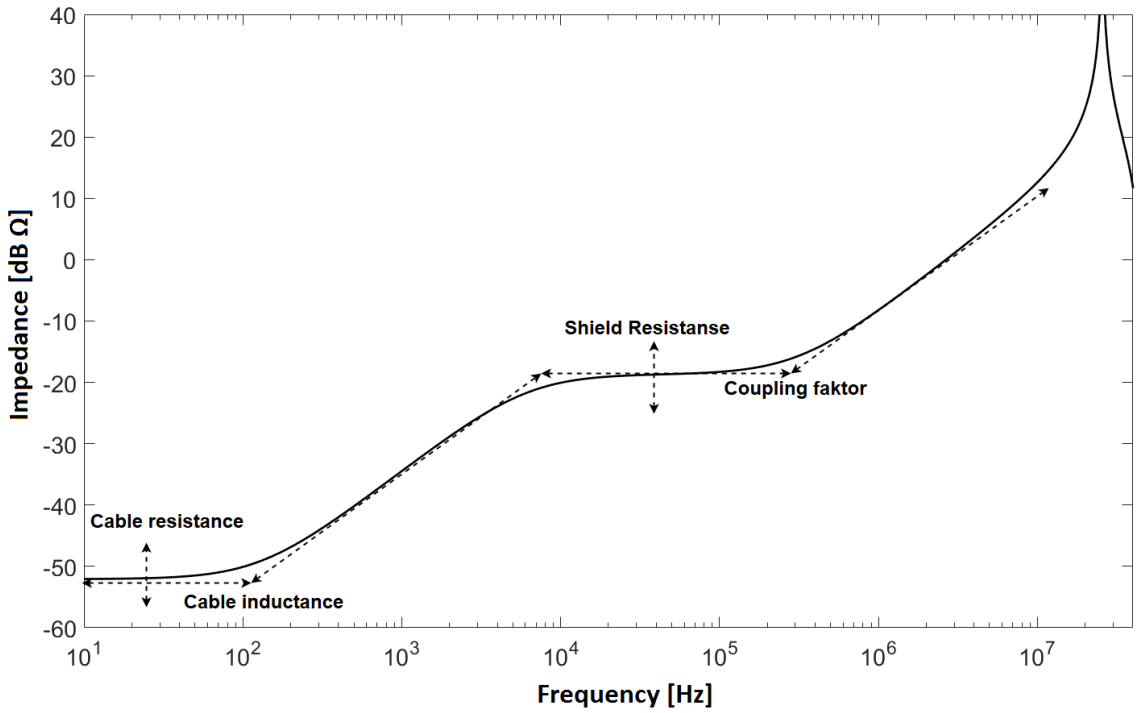

Figure 3.6: The effect of parameter change on the cable impedance.

By changing the parameters it can be observed that the impedance at low frequency is determined by the cable resistance. The impedance starts to increase when jwL_{cable} becomes dominant. If the coupling factor is large enough the impedance will then stagnate at a certain frequency interval. The length of the interval is determined by the coupling factor and its position on the Y-axis is determined by the shield resistance. This plateau behaviour is only present when the shield is connected in both ends and thus forming a loop for current to flow. The inductance which result in the increase in impedance after the plateau can be calculated as

$$L_p = L_{cable} \cdot (1 - K^2) \tag{3.1}$$

where L_p is the inductance after the plateau and K is the coupling factor.

3.7 Crosstalk Measurements

To determine the electric and magnetic fields around the cable through measurements a network analyzer is used. A line in parallel to the signal line called the victim measures voltage, transferred to it through electric and electromagnetic coupling. The procedure used is called crosstalk and measures transmission from port 1 to port 2 of the network analyser. This gives an output graph of the measured amplitude on port 2 compared to the input amplitude on port 1 for various frequencies.

3.7.1 Setup and Calibration Procedure

To preform the crosstalk measurements a standardized test rig is used. The rig consist of a copper plane with two vertical copper walls where the wires or cables can be connected as can be seen in Figure 3.7a. At the vertical copper plane coaxial cables can be connected to the network analyzer. The distance between the copper walls is exactly 1 meter.

The network analyser used is a Rhode & Schwarz Vector Network Analyser 9 kHz - 4 GHz as can be seen in Figure 3.7b. To calibrate the network analyser a closed contact is connected to the ends of the coaxial cables. The measured transmission checked so that it is 0 dB. Then an open contact is connected. This time the reflection is measured and it should be equal to 0 dB. The next test is to short circuit each coaxial cable to its outer conductor. The reflection is checked so that it is 0 dB. The final test is to connect a 50 ohm resistance between the outer and inner conductor on each of the two coaxial cables. The reflection should be very small. Finally the network analyser is calibrated using auto calibration. When this is done the network analyser can exclude the influence of the coaxial cables on the output data.

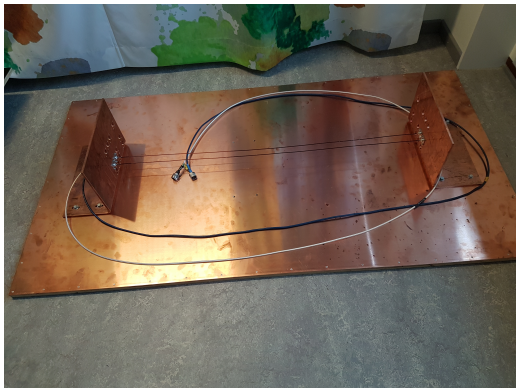

(a)

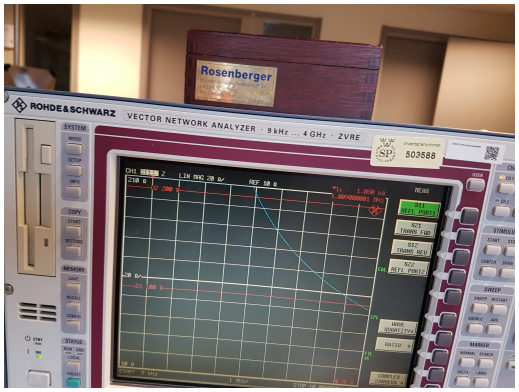

(b)

Figure 3.7: (a) The copper plane test rig and (b) the Rhode & Schwarz Vector Network Analyser.

3.7.2 Results and Comparison to Simulation Model

To compare the results of the simulations to the measurements and verifying that it matches, a setup with two parallel copper wires with a radius of 1 mm is connected to the test rig. The wires are connected to the network analyser through coaxial cables in one end and to a 50 ohm load equal to the characteristic impedance in the other end. The frequency sweep was conducted between 9 kHz to 10 MHz.

Three different cable placements were tested. The first one the two wires was placed 60 mm above ground and 30 mm between each other, the result can be seen in Figure 3.8. The second have a 60 mm height above the ground plane and 60 mm between each other. The third and last test case have a height above ground of 120 mm and a separation distance of 30 mm. The results for the second and the third test case can be found in appendix A.1.

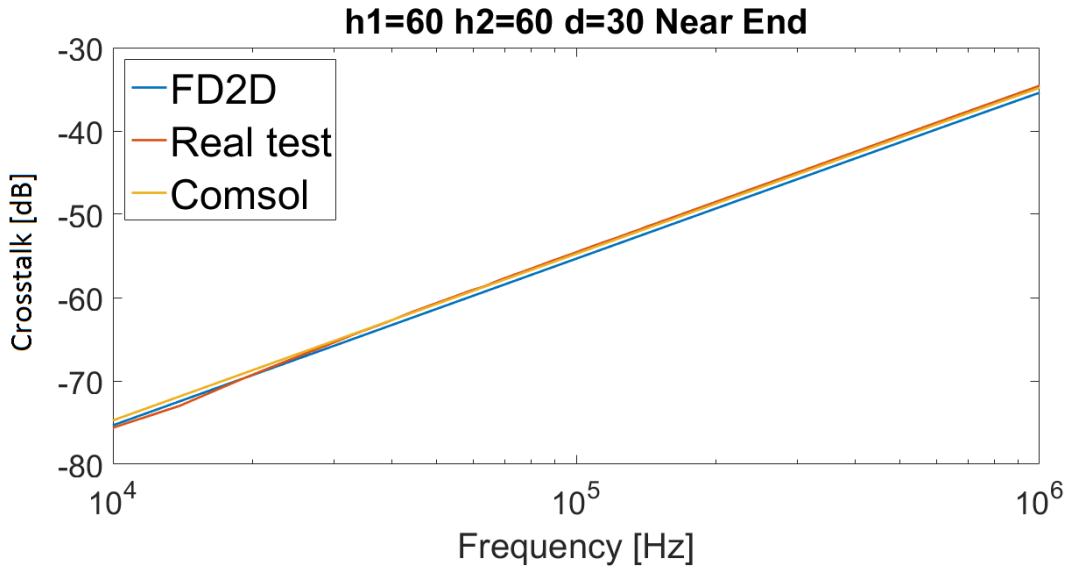

Figure 3.8: Crosstalk between two wires 60 mm above ground and 30 mm between each other.

From the results it can be noticed that the model simulation are similar to the real tests. This indicates that the model and the parameters derived from Comsol and FD2D are a good approximation of the reality.

4
Electromagnetic Compatibility

One of the main goals with this project is to reduce the electromagnetic fields emitted from the cables and thus make the cables more electromagnetic compatible. In this chapter current ripple which are the source of the magnetic fields are measured and analyzed. Then the methods of electromagnetic field reduction, mentioned in theory section 2.3 is tested using simulations and crosstalk measurements. The methods includes arrangement of the cables, twisting of the cables and shielding using various materials. The methods are tested individually and/or in combination with the other methods. Furthermore the electromagnetic force that acts during short circuit and the heat dissipation is also simulated.

4.1 Measured Harmonics in the Cables

At Chalmers a test rig of the batteries, EM, inverter and the cables have been build in order to be able to measure currents and voltages on the components for different torques and speeds. Since the current ripple are of interest, measuring the current on one of the three phase cables and one of the DC cables with a Rogowski coil, the AC component can be determined. After collecting measurement data, the Fast Fourier Transform (FFT) function in Matlab was used to observe the harmonics and at what frequency they appear.

For the first test the EM was running at a speed around 2000 rpm and producing a torque about 7 Nm. In Figure 4.1 the result of the FFT on the AC cable current can be seen. What can be noticed is the harmonics first occurs at 10 kHz while the fundamental component is at a lower frequency around 150 Hz which corresponds to 2250 rpm. The higher frequency harmonics is the cause of the inverter which uses PWM with a switching frequency of 10 kHz. It is important to note that the Rogowski coil is surrounding both the inner conductor and the shield and will therefore measure the sum of the current in both the inner conductor and the shield.

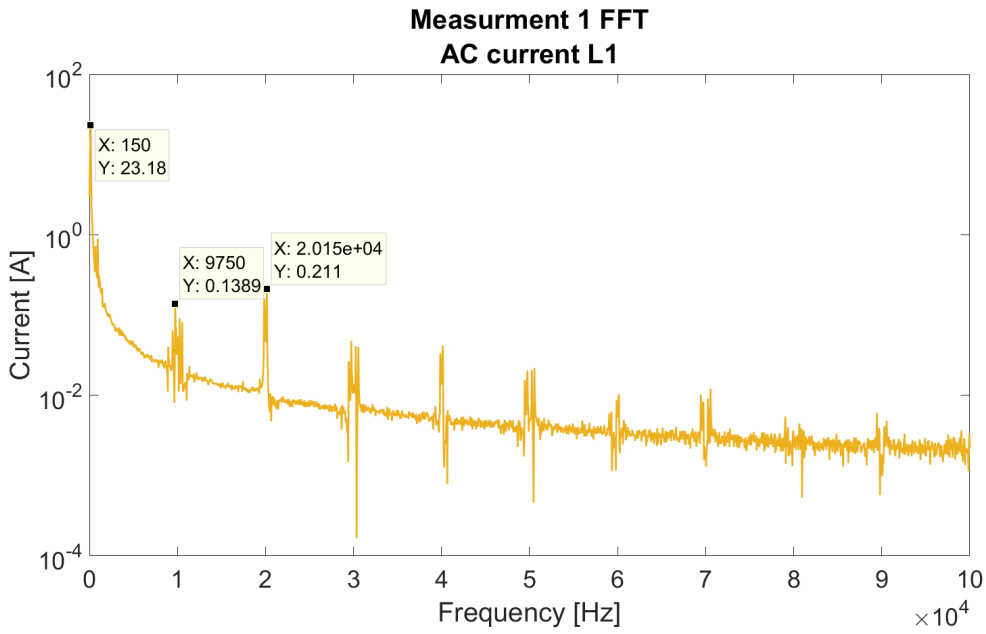

Figure 4.1: The Fast Fourier Transform of the AC current on one of the three phase cables.

The same procedure is preformed for the DC cable and the results of the FFT can be seen in Figure 4.2. Since the current was measured with a Rogowski coil the DC component will not be present in Figure 4.2, only the AC harmonics of the DC cable is shown. In this case for the DC cables, a breakout box is used so that the Rogowski coil does only surround the inner conductor. The same harmonics can be observed here from 10 kHz and above, but also a weak signal from the fundamental AC component at 150 Hz.

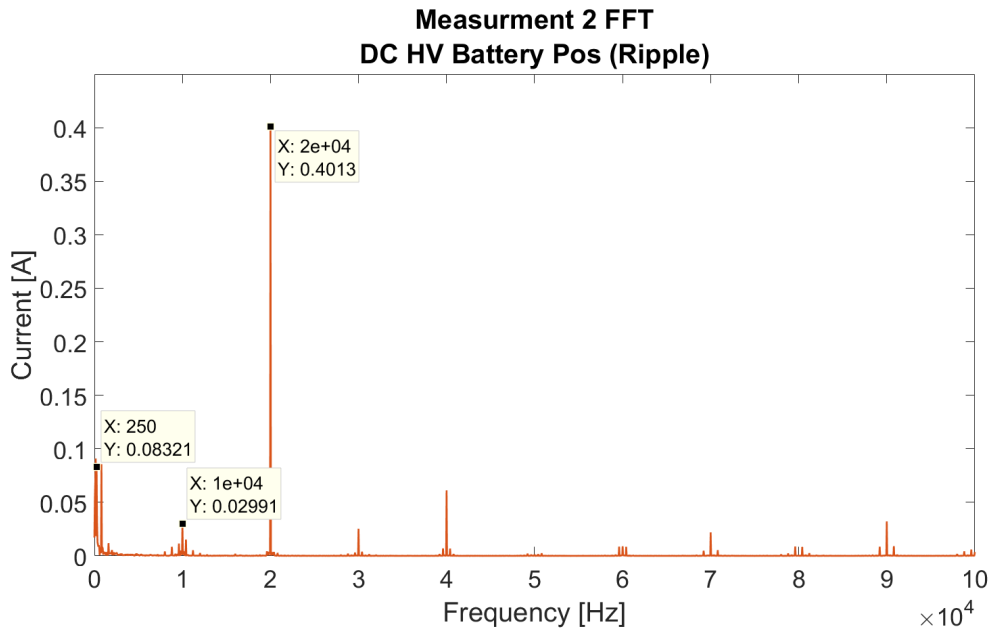

Figure 4.2: The Fast Fourier Transform of the current on the DC cable at the positive side of the battery.

This is an example for the current harmonics that can propagate during a driving scenario in the AC and DC link. These harmonics may cause EMI on the cars electrical equipment. The following sections in this chapter will present methods to reduce the magnetic field for different frequencies from 1 Hz up to 10 MHz.

4.2 Mitigation of Electromagnetic Fields

To get a better understanding of the magnetic field surrounding the cables, various Comsol simulations were performed and evaluated in order to find ways for reducing it. Almost every test is built on the FHLR2GCB2G $35mm^2$ shielded Coroplast cable. Since this is a common power cable used in the automotive industry, this cable will be the reference cable for the coming simulations. In Figure 4.3a the Comsol model of the FHLR2GCB2G $35mm^2$ shielded Coroplast cable can be seen. The parameters of the cable can be seen in Table 4.1 where the material properties of the copper and aluminum are standard values given in Comsol. The silicon rubber is made from a blank model with the material information collected from Azo Materials and J. F. Dexter and P. C. Servais report Silicone Rubber as Cable Insulation [28], [29]. While the geometry for the different layers are from the data sheet from Coroplast [30]. FHL2G $35mm^2$ cable is an unshielded cable version of the FHLR2GCB2G $35mm^2$. By using the unshielded cable together with a common shield, the geometries like the one seen in Figure 4.3b can be built.

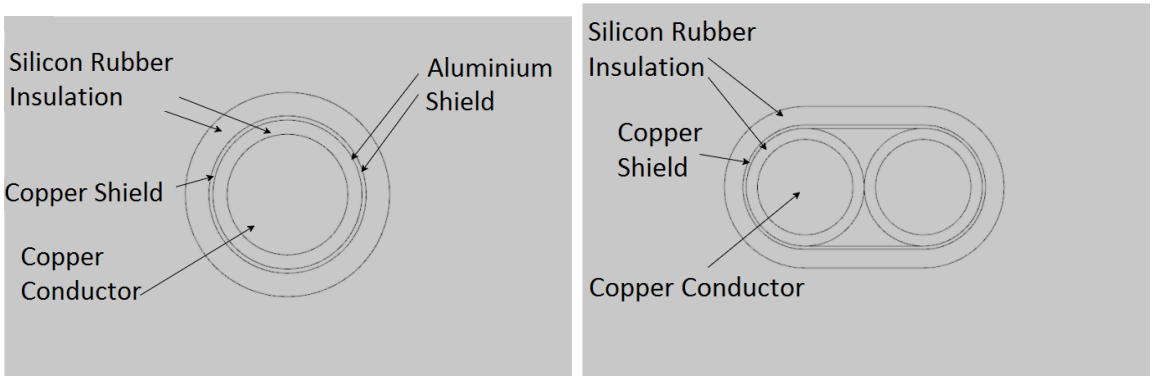

(a) **(b)**

Figure 4.3: Geometry for a a) single conductor and b) two conductors with a common shield.

In reality the shield consist of an aluminum foil together with copper wires but for the simulation a uniform copper layer is used with a thickness of 0.294 mm, equal to the thickness of both the copper wires and the foil. The reason for this is to reduce the complexity of the simulation since there seems to be no easy way to simulate the aluminum foil or the shield of copper thin wires using 2D cross section geometries. 3D geometries cannot be used either since the geometry needed is too complex to be simulated in a reasonable amount of time.

Table 4.1: The parameters for the FHLR2GCB2G $35mm^2$ shielded Coroplast cable.

	Conductor	Silicon rubber insulation 1	Aluminum 1 & 2	Copper shield	Silicon rubber insulation 2
Thickness [mm]	8.5	2	0.042	0.21	3.438
Permittivity [F/m]	1	4	1	1	4
Permeability [H/m]	1	1	1	1	1
Conductivity [S/m]	$5.9987 \cdot 10^7$	0	$3.774 \cdot 10^7$	$5.9987 \cdot 10^7$	0

4.2.1 The Shielding Affect on the Magnetic Field Mitigation

In order to get a reference on how effective a shield is, a simulation of the shielded FHLR2GCB2G $35mm^2$ and the unshielded FHL2G $35mm^2$ was preformed using the frequency domain study in Comsol. For each simulation two cables were placed next to each other with current in opposite direction. The results of the two simulations can be seen in Figure 4.4. The shield effectiveness increases at higher frequencies for the cable with the shield where as at low frequencies the shield effectiveness is non-existent. The reason for this is that the reflection and absorption losses are low at low frequencies and increases with the frequency.

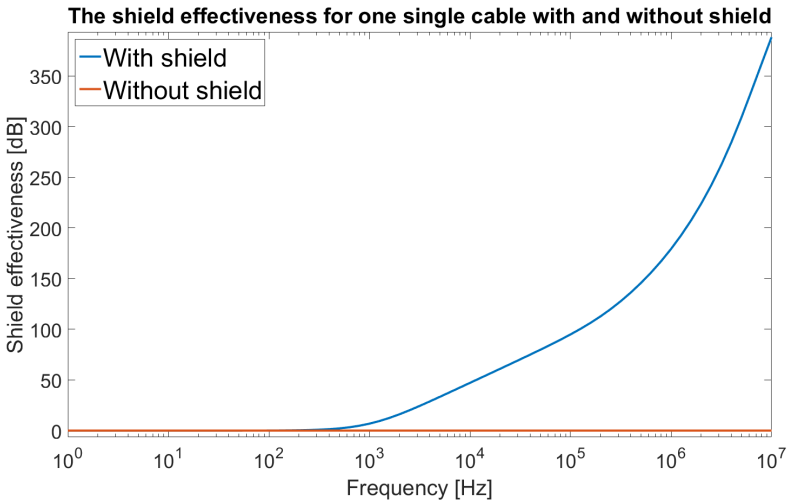

Figure 4.4: The shield effectiveness for the unshielded FHL2G $35mm^2$ cable and the shielded FHLR2GCB2G $35mm^2$.

As mentioned in Section 2.3.3, to reduce the magnetic fields at low frequencies a material with high permeability has to be used instead of a material with high conductivity. To test this the shielding material in the standard cable was replaced with mumetal. Since mumetal has non-linear permeability the material had to be implemented as mentioned in Section 3.2. Mumetal is a nickel, iron and molybdenum alloy and the parameter data is collected from the company Mushield. Mushield provides a design guide for shielding against magnetic fields. In the guide a graph is showing the permeability's behavior for different frequencies of a typical high permeability material which can be seen in Appendix A.5. This data was therefore used in order to see the effect of using a high permeability material as shield for magnetic fields [31]. The parameter data for the two different materials at 0 Hz can be seen in Table 4.2.

Table 4.2: In the table the parameters for copper and mumetal is seen.

	Copper	Mu-Metal
Permittivity [F/m]	1	1
Permeability [H/m]	1	48000
Conductivity [S/m]	$5.99 \cdot 10^7$	$1.82 \cdot 10^7$

By implementing the mumetal in Comsol and running the simulation, the shield effectiveness of the material can be measured which is shown in Figure 4.5. The figure does also include the a simulation using both a layer of copper and mumetal as well as the results of the standard shielded and unshielded cable. For the simulation with both copper and mumetal the thickness of each of the shielding layers are 0.294 mm i.e. the same thickness as the normal shield. In this case the mumetal is placed outside of the copper shield.

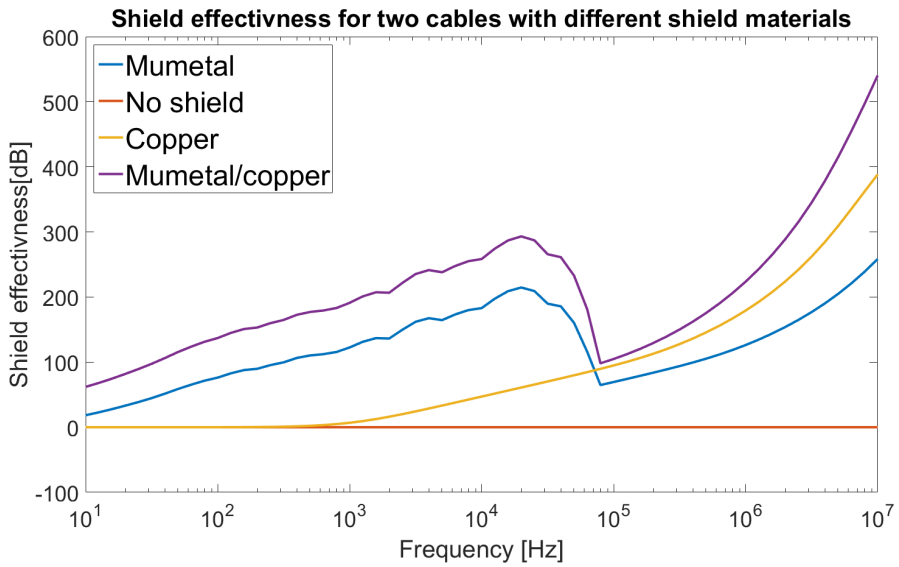

Figure 4.5: The shield effectiveness for the cable with a copper and/or a mumetal shield.

In Figure 4.5, it can be noticed that the copper shield has a very poor shielding effectiveness (SE) for frequencies below 300 Hz. The mumetal on the other hand shows good SE at frequencies below 63 kHz, because of the shunt path created in the material. However for higher frequencies the relative permeability is reduced because of its non-linear properties. Therefore it is acting as a regular conductive material though with lower conductivity than copper.

The combination of both mumetal and copper result in the best shielding effectiveness as can be expected. In higher frequencies the results can be explained as a thicker conductive shield increases the shield effectiveness. In the lower frequency range the mumetal shield is creating a shunt path for the magnetic field which induces current in the copper shield. To analyze this effect the induced current in the copper shield for the cable with the double shielding can be compared to the same induced current in the standard cable. This can be seen in Figure 4.6 where the total induced current in the copper shield is presented. The increased induced current is probably the phenomena which causes the double shielded cable to be more efficient than the mumetal shield at low frequencies.

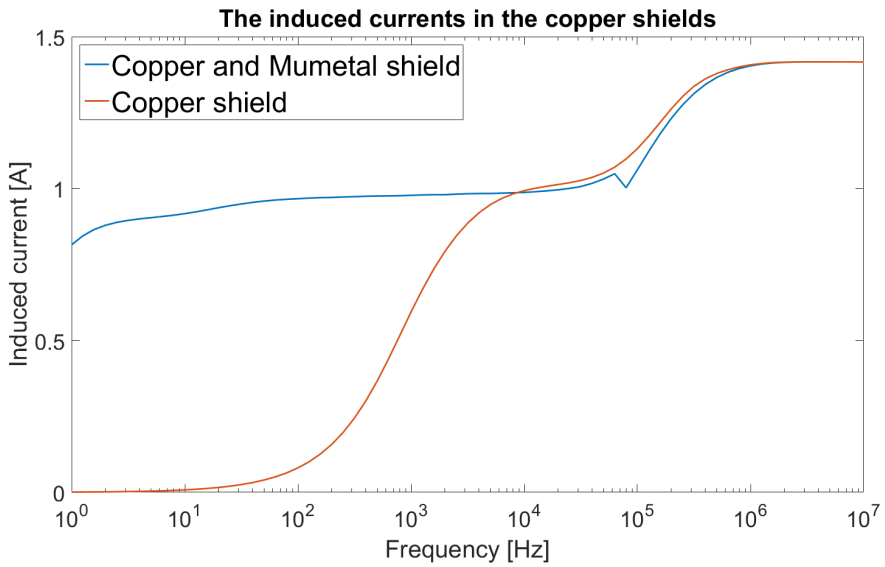

Figure 4.6: The induced current in the shield for frequencies from 0 Hz to 10 MHz.

As mentioned in the theory section 2.3.3 materials with high permeability is good for low frequencies and materials with high conductivity is better for high frequencies. This was also observed from the simulations as can be seen in Figure 4.5. In order to get a better understanding of what is happening, Figure 4.7 shows how the magnetic flux density behaves for different frequencies for the two materials, copper and mumetal. These figures are collected from the simulation with both copper and mumetal as shield. In Figure 4.7a the magnetic flux density is gathered in the high permeability mumetal material and the high conductivity copper material is not reflecting nor absorbing any fields at 10 Hz. When the frequency is increased to 10 MHz the relative permeability of the Mumetal is one and acts as a regular conductive material. The copper layer have higher conductivity and since the reflection and absorption losses is increased the magnetic flux density is gathered in the insulation and boundary between the copper and insulation layer. This can be seen in Figure 4.7b.

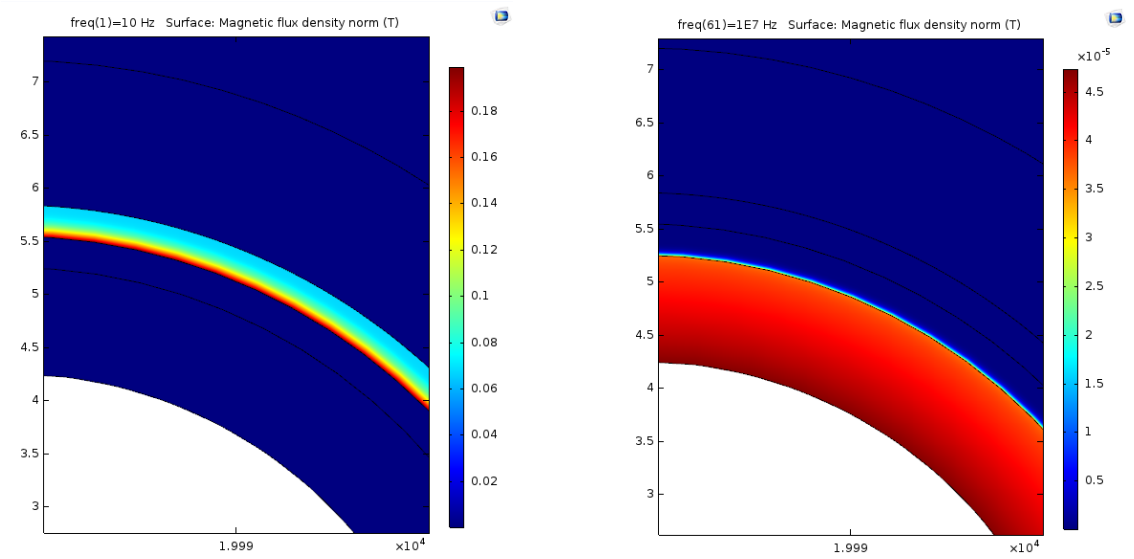

(a) 10 Hz **(b)** 10 MHz

Figure 4.7: The magnetic flux density for the copper and mumetal shielded cable at a) low frequency and b) high frequency

When to interpret the results regarding the shield effectiveness it must be taken into consideration that the model of the shield is completely uniform with ideal contact in both ends. Therefore these simulations are only to demonstrate how the shield are able to affect the magnetic field in the most ideal case. What is most interesting to read from the simulations is how the shield effectiveness varies with the frequency and perhaps not the specific values.

4.2.2 Crosstalk for Various Shield Groundings

In Comsol the shield connection is not specified since the cable is considered to be a closed loop. Therefore, to analyze how the magnetic fields are suppressed by a copper shield and how the grounding of the shield is affecting the shielding effectiveness, a series of crosstalk measurements was conducted. Channel 1 of the network analyser which generates the signal is connected to one of two parallel cables, where the cables are separated by a distance of 60 mm and placed 30 mm above ground. In the far end of the cables both ends are either short circuited or connected to each other with a 50 Ω load while the last connection at the near end is either connected to ground via a 50 Ω load or directly connected to ground which can be seen in Figure 4.8. The cables used in these measurements are 50 Ω coaxial cables.

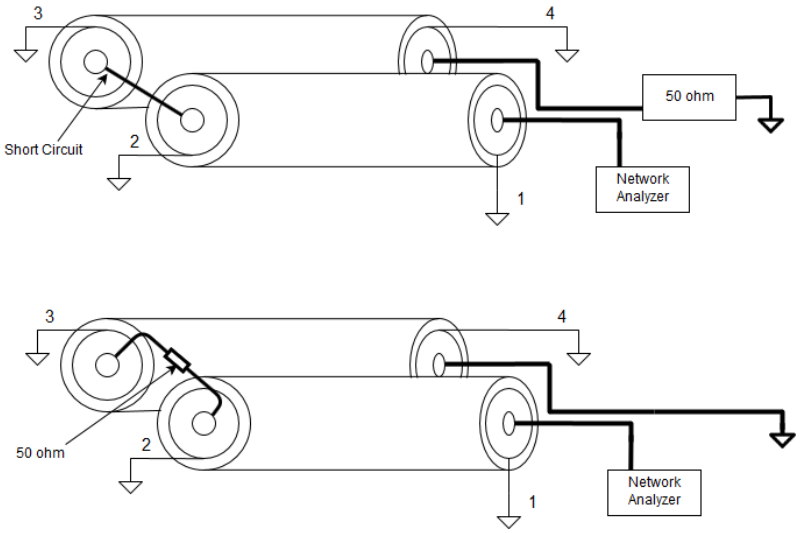

Figure 4.8: The crosstalk setup for two coaxial cables.

The measurements were repeated several times with different shield grounding connections and the results can be seen in Figure 4.9 and 4.10 where the number in the label means that the shield is grounded in that point.

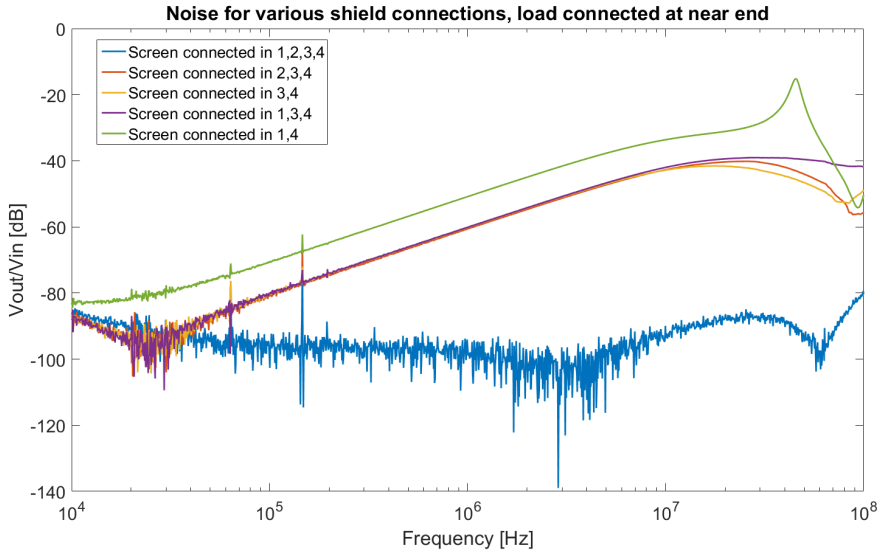

Figure 4.9: Crosstalk measurement with different shield groundings while the load is connected in the near end.

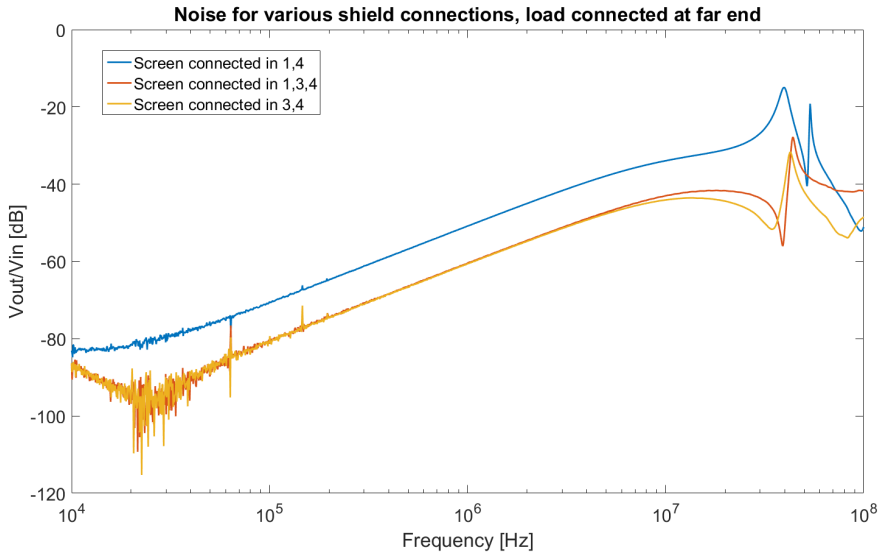

Figure 4.10: Crosstalk measurement with different shield groundings while the load is connected in the far end.

What can be observed in Figure 4.9 and 4.10 is that the shield connections affects the magnetic field significantly. The shield is most effective when all ends are grounded (1,2,3 and 4) since the current in the shields have a path to flow around both cables and creating a magnetic field which works against the one emitted by the conductors. While the one where only the same ends are grounded (1,4 or 2,3) no current will flow through the shields and therefore no magnetic field will accumulate and mitigate the conductors magnetic field. If one point at the near end and one at the far end are grounded (3,4 or 1,2) there will be current flowing through one of the shields which will create a magnetic field and therefore improving the mitigation of the magnetic field from the conductors.

4.2.3 Crosstalk Measurement with Different Cable Shields

To analyze how well the cable shields of various types of materials work in practice, a series of crosstalk measurements was conducted. The cables used in the measurements were the standard copper shielded cable together with two self-built cables containing mumetal. The cables with mumetal was made by winding a mumetal foil around the unshielded FHL2G $35mm^2$ cable. The thickness of the mumetal foil is 0.1 mm and it was winded with an overlap so that the total thickness of the mumetal layer becomes 0.2 mm. For one of the cables both mumetal and copper was used as shield, were the copper layer was made out of a braided copper wire structure. The copper were placed as the inner layer while the mumetal foil was the outer. The final insulation layer of the two cables was made out of a shrink tube.

The measurements were conducted on the copper plane test rig. Since the shield effectiveness was expected to be high, the cables were placed as high above the ground plane as possible i.e. 120 mm and with 30 mm distance to the victim. This is the setup which gives the highest possible crosstalk in the test rig. The shield was either left open in both ends or completely grounded. The results of the

measurements can be seen in Figure 4.11.

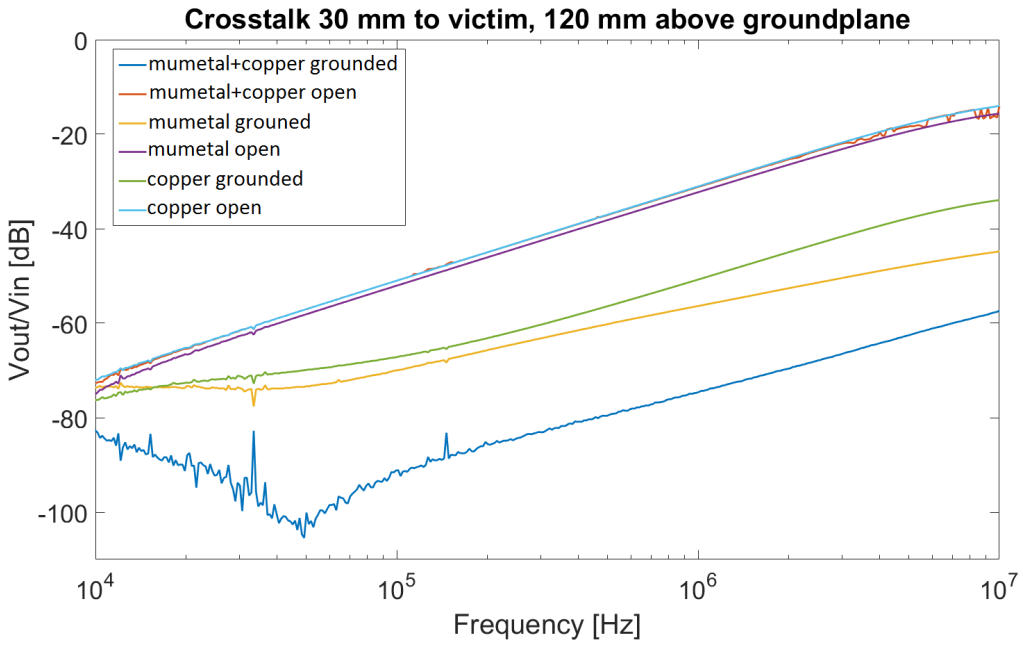

Figure 4.11: Crosstalk for shielding with copper and mumetal with either grounded or open shield connections.

From the results in Figure 4.11 it can be noticed that the cable with both mumetal and copper when grounded, has the highest shielding effectiveness in comparison to the other two cables. This was the case in the simulations also (see Figure 4.2.1). However when comparing the cable with mumetal to the cable with copper, the mumetal have higher shielding effectiveness for higher frequencies. This was not the case in the simulations. The reason for this can be that for higher frequencies the solid foil geometry of the mumetal have better affect on the magnetic field then the braided copper shield.

To find out how important the grounding is for the shield effectiveness the results in Figure 4.11 can be remade. By calculating the difference between the measured amplitude of the same cables with and without grounded shield, the importance of proper grounding can be calculated. The results can be seen in Figure 4.12, where the increased effectiveness with grounding is plotted against frequency for the three cables tested.

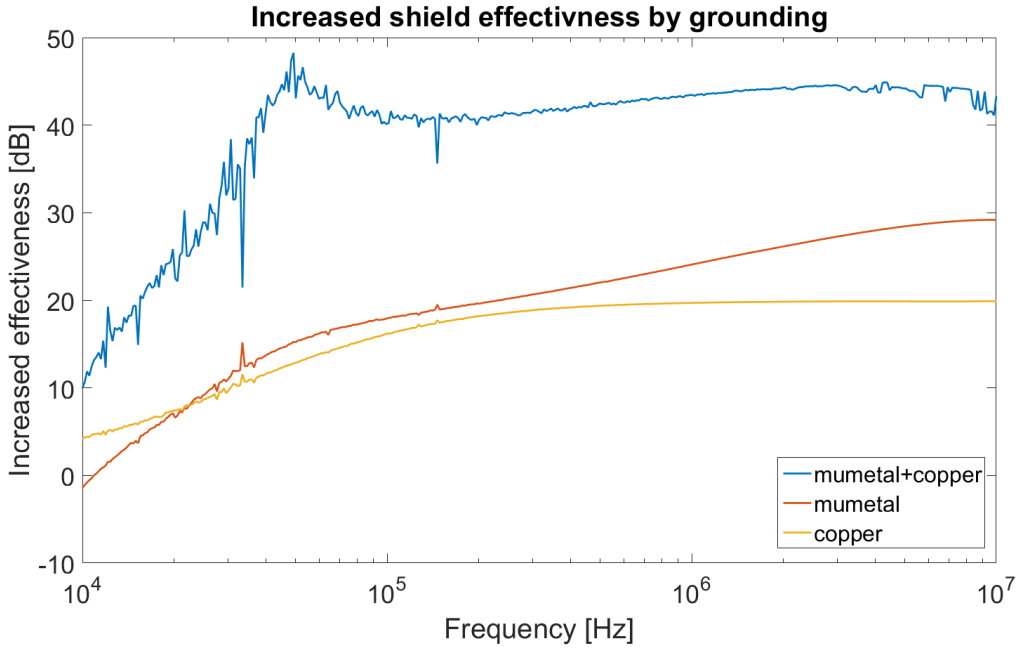

Figure 4.12: Increased effectiveness of copper and mumetal shields by grounding.

Since the mumetal shield is most effective at low frequencies and the network analyzer cannot measure lower than 9 kHz, a new measuring method was necessary. By using a oscilloscope and a signal generator, the crosstalk for frequencies from 10 kHz to 100 Hz could be measured. By applying a signal to the cable and then measuring the voltage on the victim line with a oscilloscope the transferred gain could be calculated. The first measurement was conducted with the standard cable which have a copper shield and the test was done with the shield grounded and open. The results can be seen in Table 4.3.

Table 4.3: The crosstalk measurement for the standard cable with a copper shield

	10 kHz	5 kHz	2 kHz	1 kHz	500 Hz	250 Hz	100 Hz
Open [dB]	-71.08	-77.18	-85.01	-90.52	-95.68	-96.80	-103.35
Grounded [dB]	-76.30	-79.75	-85.99	-91.40	-96.97	-97.89	-102.99

Second test was to use the FHL2G $35mm^2$ cable but with a mumetal shield around it and the results are presented in Table 4.4.

Table 4.4: The crosstalk measurement for the FHL2G $35mm^2$ cable with a mumetal shield.

	10 kHz	5 kHz	2 kHz	1 kHz	500 Hz	250 Hz	100 Hz
Open [dB]	-71.04	-77.15	-84.93	-90.70	-96.30	-100.32	-103.35
Grounded [dB]	-79.13	-81.44	-86.55	-91.49	-96.80	-100.07	-106.34

The third and last test was with the FHL2G $35mm^2$ cable with a copper shield and with a second shield of mumetal around it. Table 4.5 shows the results.

Table 4.5: The crosstalk measurement for the FHL2G $35mm^2$ cable with a mumetal and copper shield.

	10 kHz	5 kHz	2 kHz	1 kHz	500 Hz	250 Hz	100 Hz
Open [dB]	-71.10	-77.22	-85.06	-90.70	-95.68	-98.91	-
Grounded [dB]	-95.53	-102.32	-108.03	-	-	-	-

By comparing the results from the three different test it can be noticed that the grounding of shield is important even for low frequencies. As expected the mumetal shield is mitigating the magnetic field better than the copper shield for low frequencies. The copper and mumetal shielded cable shows the best shielding properties in comparison to the other two cables for the whole frequency spectrum. This was also seen in the simulations in section 4.2.1. Note that the amplitude of the signal is very weak and close to the noise floor in the low frequency range. The measurement is therefore not very accurate in this range but it follows the same pattern as seen in the simulations.

4.2.4 The DC Link Cable Arrangement

The cable arrangement can also affect the surrounding magnetic fields. Therefore different arrangements will be tested and evaluated. The first test is to evaluate how the magnetic field is affected depending on if a common shield or separated shields are used for the two cables. The geometry for the common shield cable used can be seen in Figure 4.3b. In Figure 4.13 the test results are presented for both separated and common shielded cables. In both simulations the cables were placed as close as possible.

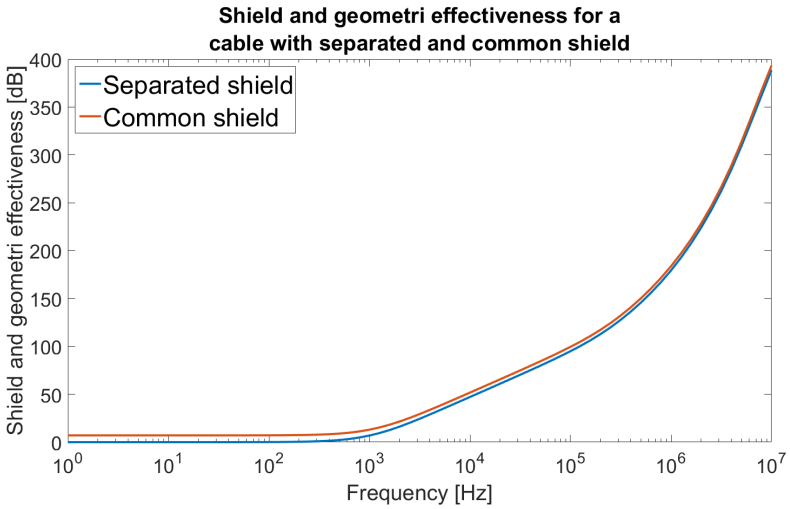

Figure 4.13: The shield effectiveness FHLR2GCB2G $35mm^2$ shielded Coroplast cable with separated shields and FHL2G $35mm^2$ cable with a common shield for different frequencies.

The results seen in Figure 4.13 shows that the common shield have an improved shield and geometry effectiveness for frequencies from 1 Hz to 10 MHz. The increased

effectiveness with common shield varies between 7 dB to 4 dB within this frequency span. The reason for this is that the conductors are placed closer together with the common shield arrangement and therefore the magnetic fields emitted by the cables have a higher cancellation effect.

Since simulations indicates that the common shield is good for reducing magnetic fields, more cable arrangements were tested. The different geometries that have been tested and evaluated for reducing the magnetic field can be seen in Figure 4.14. To be able to compare these geometries the same parameters as for the standard cable (see Table 4.1) was used.

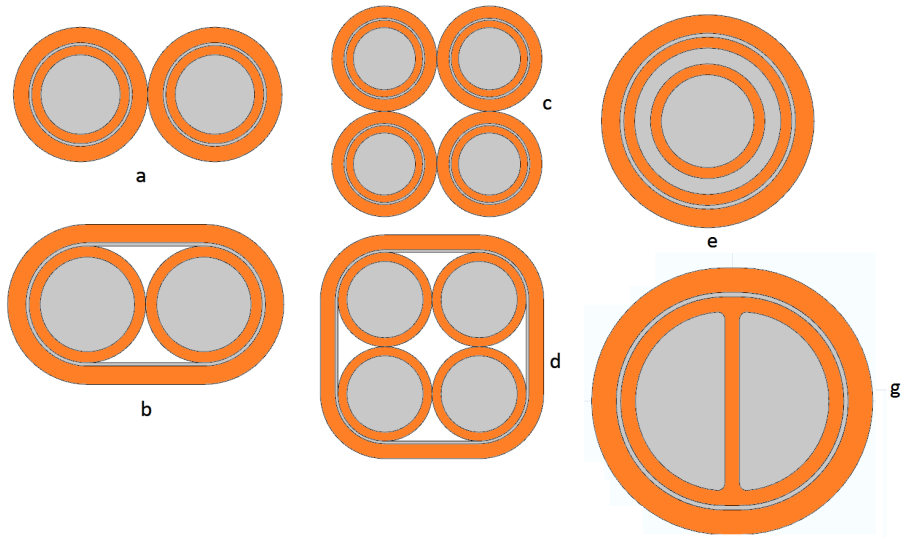

Figure 4.14: The geometries for the cables with different setups, a) standard two cable with separated shield, b) two cables with a common shield, c) four cables, d) four cables with a common shield, e) one cable with the second conductor around it and g) a multicore cable with a common shield

A frequency domain study was preformed for each one of the cable arrangements in Figure 4.14. For the arrangements with two cables for each phase i.e. c and d the current for each cable is divided by two. Each phase are then placed diagonally. The results of the simulations can be seen in Figure 4.15. In Table 4.6 level of geometry and shield effectiveness can be seen for a few specific frequencies.

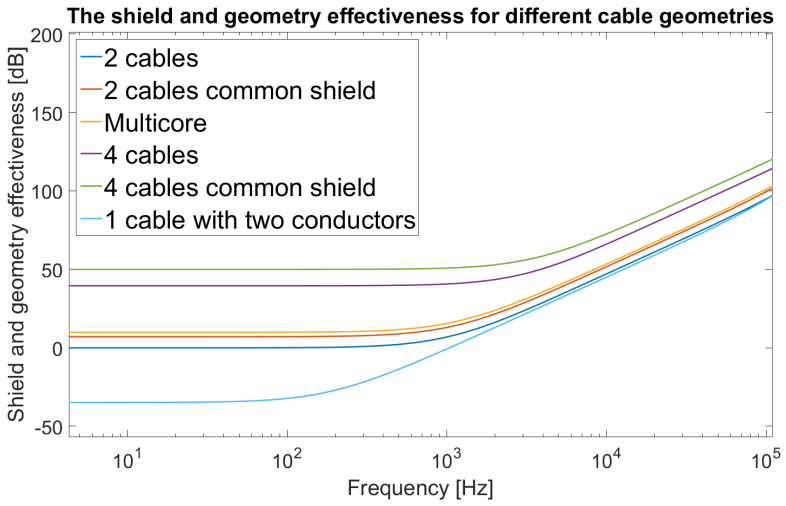

(a)

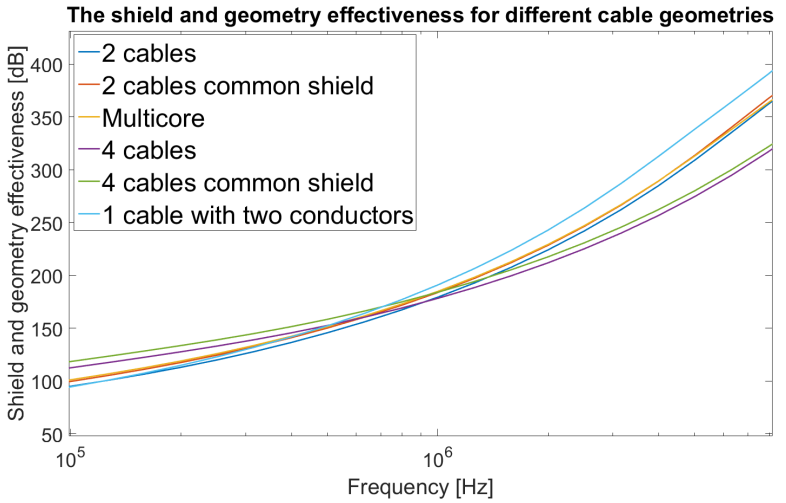

(b)

Figure 4.15: The shield and geometry effectiveness for the different geometries a) for frequencies up to 100 kHz and b) up to 10 MHz

Table 4.6: The shield and geometry effectiveness for the different DC cables.

Shield & geometry effectiveness [dB]	10 Hz	100 Hz	1 kHz	10 kHz	100 kHz	1 MHz	10 MHz
2 cables	0	0.06237	6.853	47.12	94.93	179.3	388.4
2 cables Common shield	7.024	7.114	12.96	51.71	99.49	183.7	393.3
Multicore	9.846	9.928	15.53	53.41	101	184.7	388
4 cables	39.55	39.56	40.67	66.07	112.4	178.2	341.3
4 cables Common shield	50	50	50.81	72.56	118.4	183.9	344.4
1 cable with 2 conductors	-34.84	-32.28	-0.688	45.07	94.37	190.8	419.1

By looking at Figure 4.15 it can be noticed that the magnetic fields can be reduced by splitting up the phase and placing the phases diagonally compared to only using two cables as for arrangement a. The reason this works is that a greater cancellation effect can be achieved with four cables. However this effect is only present up to 1 MHz. As previous simulations has shown the common shield for the cables reduces the magnetic fields around the cable. The result in Figure 4.15 shows that this is the case for arrangement c and d as well.

Arrangement g, the multicore cable was showing the best results of the cable arrangements with two cables. If there is no possibility of using more then two conductors for each phase this would be the choice for a good field reduction for frequencies from 0 Hz to 10 MHz. The conductors in this arrangement are placed even closer to each other and the field cancellation effect is therefore improved even further than for the arrangement b. The same setup could be used for four conductors. This have not been tested since it will very likely have the same effect as with the four cable setup but with a slight reduced magnetic field since the conductors are closer to each other.

Arrangement e had the worst field reduction at low frequency of all the arrangements tested. This arrangement was even worse than the free conductors which acts as the reference. However for frequencies above 1 MHz it is superior to all the other arrangements. The reason for this could be that the absorption and reflection losses are increased. This since the second conductor work as a second shield. However the simulations results are more uncertain at higher frequencies, since the shield is simplified. Therefore this might not actually be the case.

4.2.5 The AC Link Cable Arrangement

The AC link in the vehicle is a 3-phase system. Therefore, as mentioned in 3.2 the magnetic flux must be measured over a whole period so that the average values of the flux can be derived. The AC link geometries used is quite similar to the DC link arrangements, except that there is three phases instead of two. The geometries tested can be seen in Figure 4.16. As for the DC link, splitting up each phase, common shield and the Multicore arrangements was used. Since the magnetic field

is reduced if the cables are closer to each other a triangle delta arrangement of the cables are also tested.

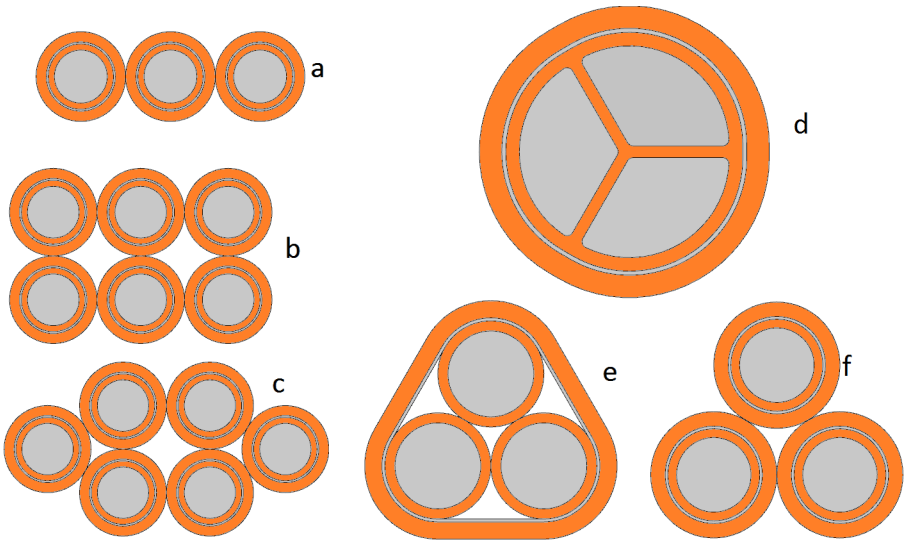

Figure 4.16: The geometries for a) standard 3 cables lying flat, b) 6 conductors with each phase split in to two and lying flat, c) 6 conductors placed tighter as a hexagon, d) multicore cable where the conductors are triangle shaped, e) triangle formation with a common shield and f) triangle shape with separated shield

For the arrangement b and c with a total of six cables the phases can be assigned in different ways. To determine which way that gives the highest field reduction, the phase arrangements that was most likely to give the best cancellation were tested. The results of the test can be seen in Figure 4.17. It can be observed that for higher frequencies all the different arrangements are almost the same but at lower frequencies the best arrangement seems to be when placing each conductor in series one after another and creating a rather symmetrical phase arrangement. The first row from the left will be a,b then c and the second row from the left will be c,b then a. This will therefore be used in the simulations when comparing different geometries.

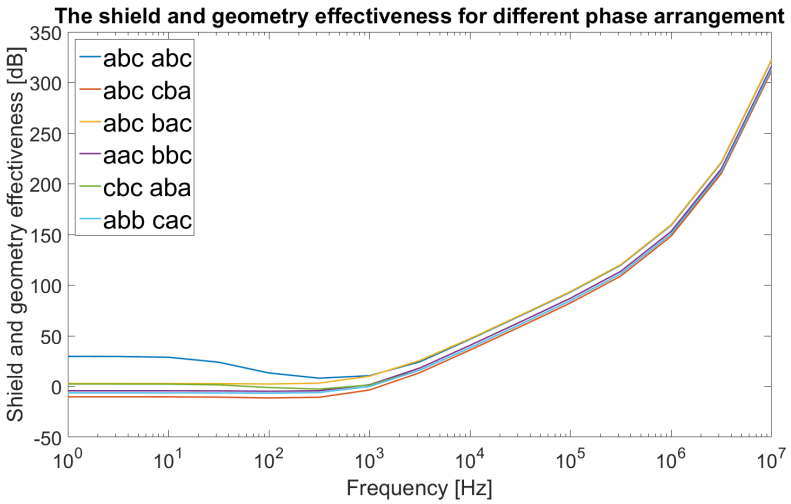

Figure 4.17: The shield and geometry effectiveness for different phase arrangements with two conductors for each phase.

To test and compare all the cable arrangements a simulation was preformed for each one of the arrangements. For the arrangements with six cables phases are arranged abc abc since this gives the best field reduction (see Figure 4.17). The results of the shield and geometry effectiveness can be seen in Figure 4.18. In Table 4.7 the exact values for a few specific frequencies is shown.

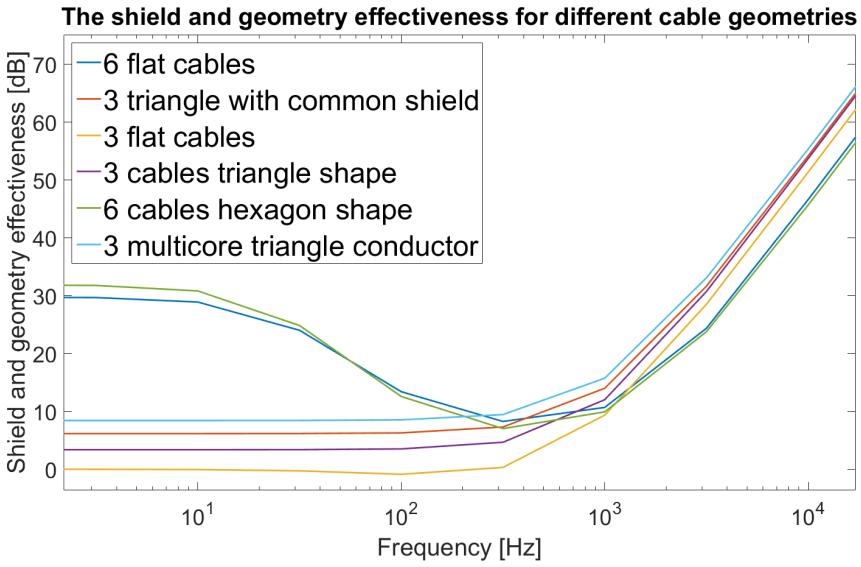

(a)

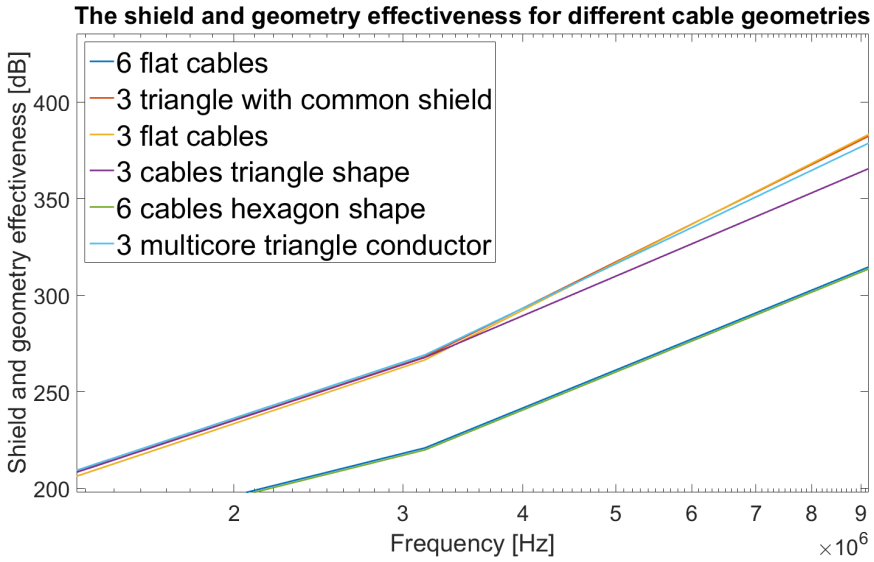

(b)

Figure 4.18: The shield and geometry effectiveness for all the different arrangements a) for frequencies up to 10 kHz and b) up to 10 MHz

Table 4.7: The shield and geometry effectiveness for different three phase cables.

Shield & geometry effectiveness [dB]	10 Hz	100 Hz	1 kHz	10 kHz	100 kHz	1 MHz	10 MHz
3 flat cables	0	0	9.316	51.35	99.16	183.5	392.7
3 cables triangle shape	3.342	3.477	11.99	53.68	101.5	185.8	373.3
3 cables triangle shape with common shield	6.124	6.247	13.96	54.18	102	185.8	391.6
Multicore triangle shape	8.391	8.498	15.7	55.33	103	186.8	387.6
6 flat cables	28.87	13.37	10.65	46.6	93.22	159	322.2
6 cables hexagon shape	30.79	12.55	9.886	45.65	92.26	158	321.1

As can be seen in Figure 4.18 the six conductors set ups shows great properties for frequencies up to 300 Hz. However for higher frequencies the magnetic field reduction is very poor compared to the regular setup a. The best geometry over all seems to be the triangle setups or the Multicore. This is because the conductors are placed very symmetrically and close to each other, the cancellation effect is therefore greater than the standard flat setup. Common shield for six conductor was not tested but the results can be expected to be similar as for the triangle shape.

4.2.6 Twisting the Cables and its Affect on the Magnetic Field

Another way to reduce the magnetic field radiated by the cable is to twist the cables. Simulating 3D twisted cables and its magnetic field in Comsol demands a huge amount of performance therefore this report will only include analytic calculations for twisted cables and its affect on the magnetic field. In section 2.3.1 in the theory chapter a very approximate solution for calculating the magnetic field with and without twisting the cables is seen. By calculating the effective value of the magnetic field with (2.38) and using a=1 mm, I=200 A, r=0.1 m and p=1 m as parameter values, the effective value of the magnetic field for the untwisted cable can be calculated to 8μT. For the twisted cable using (2.43) the value can be calculated to 2.66μT which is a 67% reduction. This shows with the information from other articles and reports that in order to mitigate the magnetic field radiated from the cables, twisting the cables can be a quick and cheep solution.

4.2.7 Cable Separation and its Affect on the Magnetic Field

All previous simulations has been preformed with the cables placed as close together as possible. Therefore in order to understand how the distance between the cables affect the magnetic flux density a parametric sweep of the separation distance was preformed in Comsol. The magnetic flux density was measured at the distance 100 mm to the right of the right conductor and 100 mm above both conductors. The simulations was done with the cable model of the shielded Coroplast cable which

was placed 120 mm above a ground plane and applied with a DC current, the results can be seen in Figure 4.19.

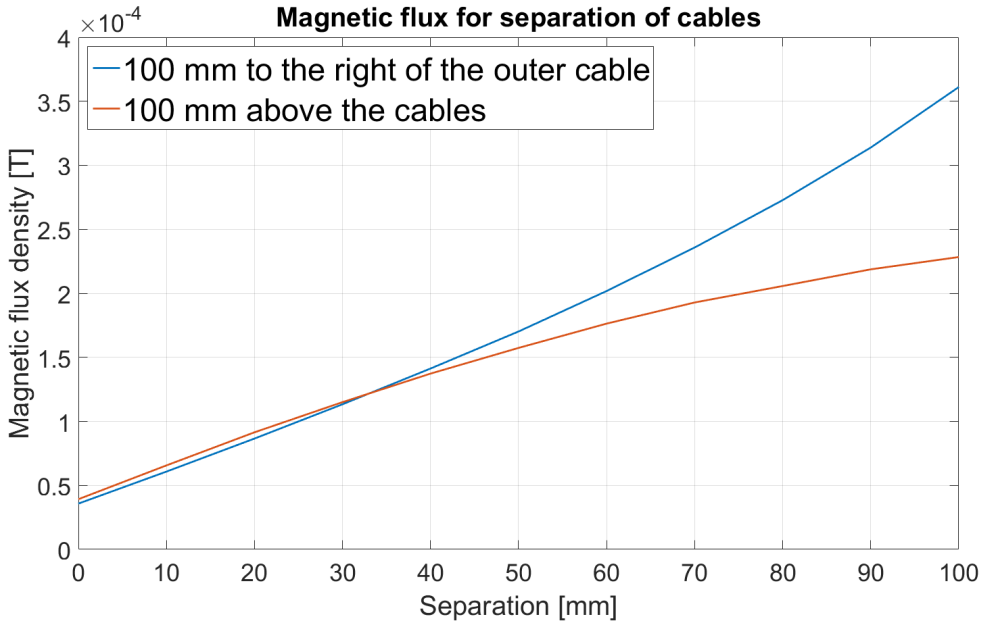

Figure 4.19: Magnetic flux density for separation of the cables.

It can be noticed in Figure 4.19 that the magnetic flux density increases about 10 times with a separation of 100 mm compared to no separation when measured to the right of the cable. The magnetic flux density above the conductor also increase with the separation distance. The pace of the increase however is not as high.

To see how the fields behave in practice a crosstalk measurement on a RG58 coaxial cable was conducted with the copper plane test rig, the results can be seen in Figure 4.20 and what can be observed is that the amplitude of the measured signal increases with a increasing separation between the cables. Which confirms results from the Comsol simulation.

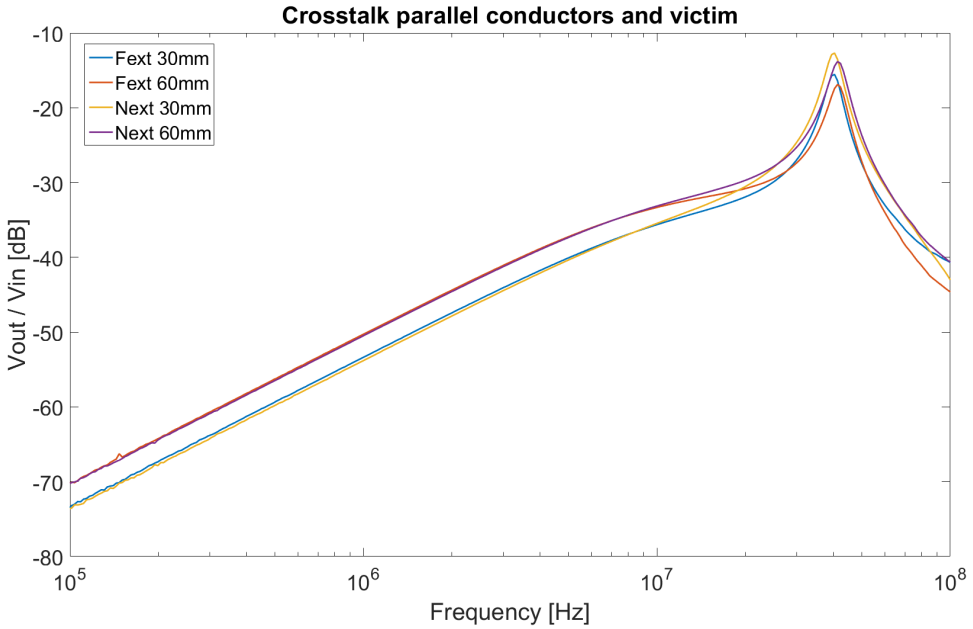

Figure 4.20: The V_{out} / V_{in} gain for the RG58 coaxial cable with different separation distances.

4.3 Magnetic Force During Short Circuit

As mentioned in the theory chapter section 2.4, when current flows through a conductor a force occurs which is proportional to the current square for parallel conductors. The short circuit current from the battery pack in the Volvo XC90 can reach up to 5000 A under 12 ms and by using Comsols function of electromagnetic force, the force can be calculated to 346.89 N/m acting outwards on the cables as seen in Figure 2.4.

The calculated force are in the worst case scenario since the current applied in the simulation is the maximum current the battery can deliver and the cables are placed as close as possible. Since the cables are placed in cable casings the force is probably not high enough to cause any damage. However if the short circuit current from the battery is increased it may be able to cause damage during short circuit faults.

4.4 Possible Issues with New Cable Arrangements

If a new cable arrangement is used a number of issues may occur. One of these issues can be that when using a common shield there is only one protective layer of insulation between the conductors. Therefore, when the cables are used in the car the cables will scrape against each other, which may damage the insulation in the long run. The chance for a short circuit is therefore increased compared to the standard cable where there are two insulation layers and a copper shield layer in between the inner conductors.

When looking at materials for the cable shielding, especially mumetal, the price is an important factor. When ordering the materials for the cables which were tested in the copper plane test rig, the first thing that was noticed was the price for mumetal is much higher than the price for the copper shield. Therefore manufacturing cables with mumetal shields will be more expensive than cables with copper shields.

Another issue may be the temperature development in the cable. By using different geometries such as the common shield setup, the temperature in the cable will change since the conductors are closer and therefore have less thermal convection. This since there will be less air flow around the cables to cool them down. The temperature of the cable can therefore be an important factor to determine if the different geometries are possible to implement or not.

To analyze this a couple of tests was conducted in Comsol. Since Comsol now is solving for thermal heat transfer, new parameters for the materials is required. The thermal properties used for air and copper is already implemented in Comsol. However silicon rubber is made from a blank material with the parameters in table 4.8.

Table 4.8: Thermal material properties [2].

	Copper	Silicon Rubber
Density $[kg/m^3]$	8960	1420
Thermal Conductivity $[W/(m \cdot K)]$	400	0.2
Heat Capacity $[J/(kg \cdot K)]$	385	1733

By looking at the given datasheet for the FLR2GCB2G 35 mm^2 cable from Coroplast it can be noticed when applying 150 A, the core temperature is just under 50 °C while in the simulation it is around 45 °C. The difference could depend on how the data from the datasheet was collected, in Comsol the temperature went to steady state after 133 minutes which can be seen in Figure 4.21. The model made in Comsol is therefore taken to be a quite good model to use for further tests [30].

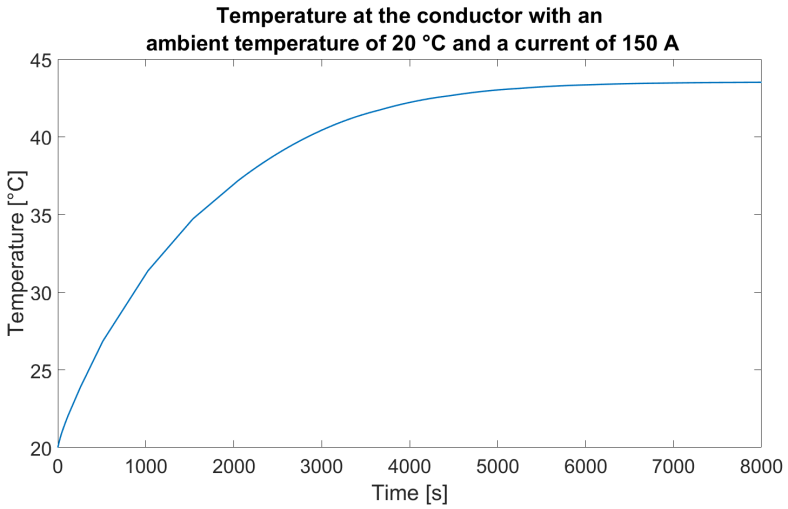

Figure 4.21: The conductor temperature for a single cable applied with 150 A at an ambient temperature of 20 °C.

The second test was to try out the temperature of the common shield geometries that looked promising seen in Figure 4.15a. By using a common shield around the conductors there would be no airflow to cool the cables down and the heated air is trapped inside of the cable which would therefore lead to a increase in temperature. The results from the test are seen in Figure 4.22 and 4.23, what can be observed is that the common shields have an increase in conductor temperature, particularly the ones with two conductors. Probably because the area for the heat to dissipate in is smaller compared to the one with four conductors.

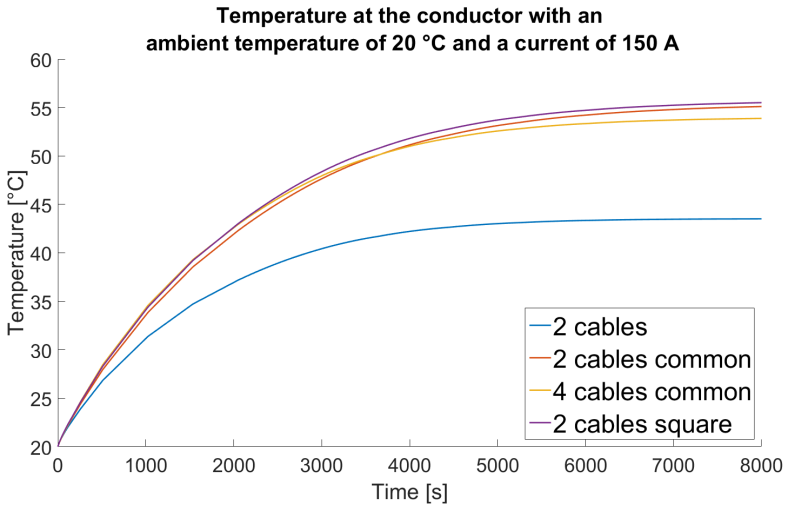

Figure 4.22: The conductor temperature for the standard cable setup, two cables with a common shield and four cables with a common shield applied with 150 A at an ambient temperature of 20 °C.

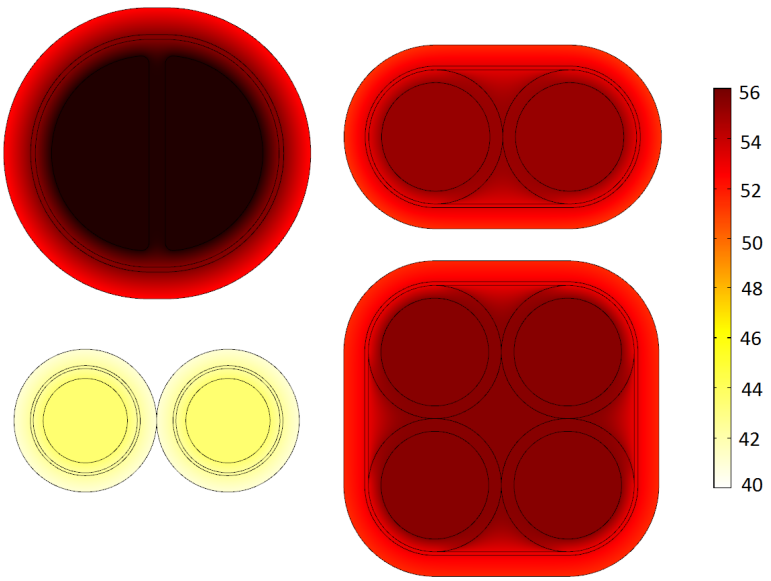

Figure 4.23: The cable temperature for three different geometries with the ambient temperature of 20 °C and an applied current of 150 A

5
Cable Parameters

In this chapter the cable parameter will be determined using both simulations and measurements. The results will then be compared and analyzed in order to get a deeper understanding of how the geometry and frequency affects the results.

5.1 Inductance Measurements

The inductance for the cables can be measured by creating a resonant circuit, measuring the resonant frequency and calculating the inductance by using (2.18). The resonant frequency is measured by preforming a frequency sweep and identifying the resonant peak. In this study the inductance will be calculated for both long cables to get accurate inductance per length and for the cables used in Volvo XC90 connected to its contacts.

5.1.1 Setup and Calibration Procedure

The circuit used for the inductance measurement consist of the cable in series with a capacitor with a known capacitance. Voltage is applied over the circuit and measured by a network analyzer at the node in between the cable and the capacitor as can be seen in Figure 5.1.

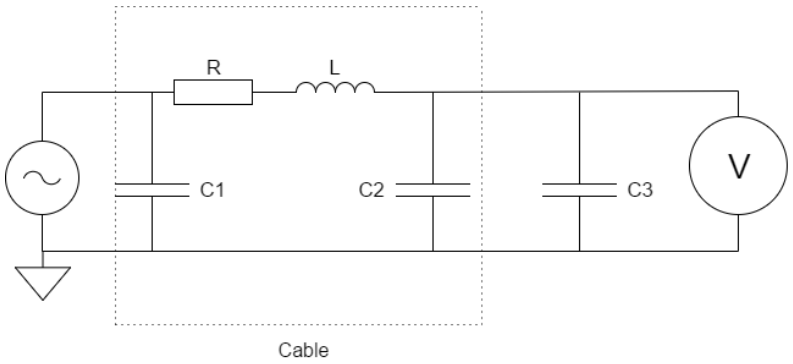

Figure 5.1: Pi model of the cable with the measuring setup.

In Figure 5.1, the voltage source on the left and the voltage meter which on the right is in this case a Omicron Bode 100 network analyser. The dotted box in the figure is the pi model of the cable. C3 is the capacitor added to the circuit to create resonance and in order to determine what size of the capacitor to use a

few simulations was preformed in LTSpice. Since the Bode 100 is limited to 40 MHz, a too small capacitance will put the wanted resonant peak over 40 MHz and to large capacitance will result in a less distinct resonant peak according to the LTspice simulations. Therefore 330 nF was chosen to be a suitable size for these measurements.

To calibrate the Bode 100 network analyzer the same procedure as for the Rhode & Schwarz Vector Network Analyzer with through, open, short and load connectors at the coaxial cables was preformed. The output voltage will therefore be measured at the point where the coaxial cable enters the contact circuit. In Figure 5.2 the contact circuit is shown.

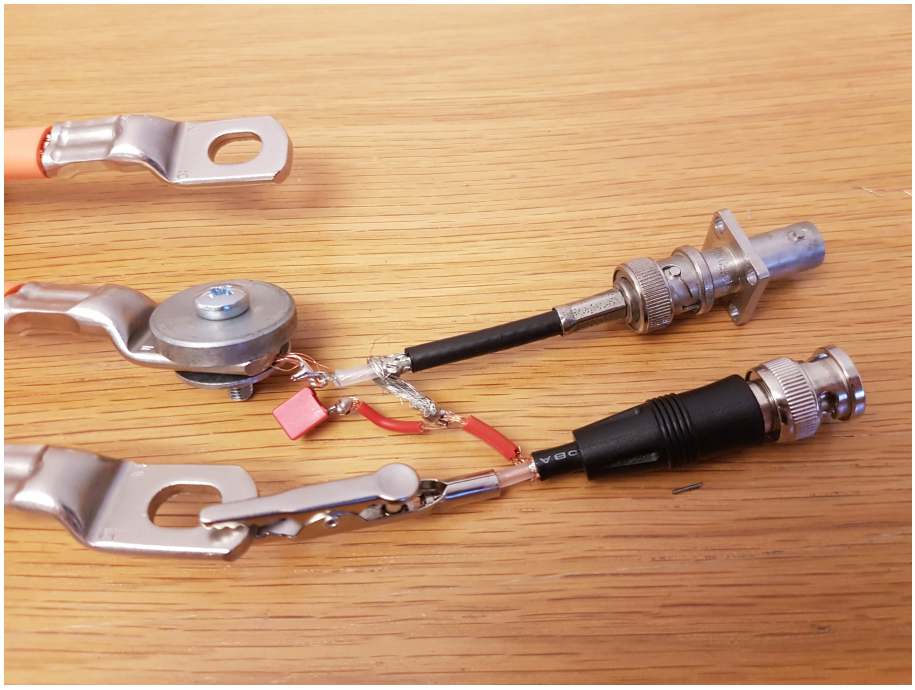

Figure 5.2: The contact circuit with the 330 nF capacitor for measuring the inductance of the cable.

Before the inductance of the cable could be measured a measurement on only the contact circuit were preformed where the contact points that should be connected to the cable are short circuited. This is done so that the inductance of the contact circuit can be subtracted from the actual measurements.

5.1.2 Inductance Measurements on the Different Cables Setups

To get accurate inductance per meter measurements a 10.15 meter long standard shielded cable and a 10.4 meter long unshielded cable was used. Also for the common shield cable a four meter long piece was tested, the shortness of the cable was because of the limiting resources which meant only four meters could be crafted. The cables were connected to the measurement circuit illustrated in Figure 5.1 and the non-common shielded cables were placed with both a 7 and 0 cm separation. For each

separation the shield was either grounded in both ends or not grounded at all. In Figure 5.3 the placement for the standard cable with 7 cm separation can be observed.

Figure 5.3: Placement setup for the $35mm^2$ shielded Coroplast cable with 7 cm separation.

The results from the measurements for the standard cable can be seen in Figure 5.4 while the results for the shield of the cable, the unshielded cable and the common shielded cable can be found in appendix A.2.

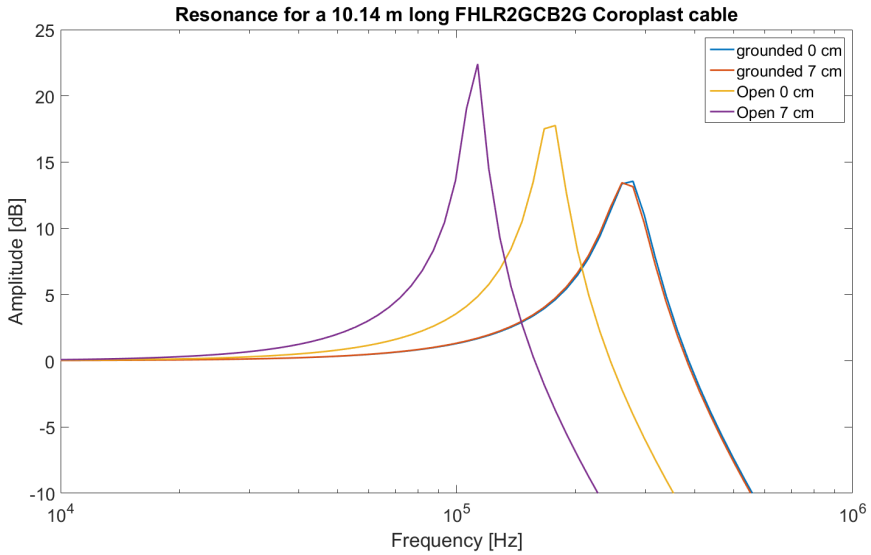

Figure 5.4: Resonant frequency measurement for a 10.14 meter long FHLR2GCB2G $35mm^2$ Coroplast cable.

From Figure 5.4 the resonant frequency can be identified as 113 kHz with 7 cm separation and as 172 kHz with 0 cm separation when the shield is open. When the shield is grounded the resonant frequency is instead 270 kHz for both 7 and 0 cm separation. By inserting the resonant frequency and the capacitance of 330 nF to (2.18) the inductance can be calculated. The results of the derived inductance per meter for the cables can be found in Table 5.1.

Table 5.1: Measured inductance for the different cables.

Cable configuration	Open 0/7 cm $[nH/m]$	Grounded 0/7 cm $[nH/m]$	Twisted cables 1 turn/m $[nH/m]$
Shielded cable	246 / 583	94.3 / 94.3	-
Shield inductance	176 / 512	-	-
Common shield	105 / -	105 / -	-
Unshielded cable	197 / 606	-	184

In Table 5.1 open means that the shield is not grounded for the shielded cables and that the inner conductor is not connected regarding the shields inductance. For the free conductors it does not mean anything since there are no shield to connect. The length of the cable with common shield is four meter long so the uncertainty of the results is slightly higher regarding that measurement. The reason why some columns are unfilled are because these geometries are not definable or not tested.

One of the most interesting results from the measurements is that grounding of the shield greatly affects the inductance of the standard shielded cable. Furthermore it is also interesting that the separation distance does not affect the inductance when the same cable is grounded. However the same thing is not true for the common shielded cable. In this case the grounding of the shield does not affect the results at all. It is worth mentioning that the shield of the common shielded cable only was connected to ground in one end.

5.1.3 Inductance Measurements on the Standard Cable with Contactors

To measure the inductance of the cable together with the contactors the cable were placed on a wooden table and connected to the same contact circuit as for the long cables measurement seen in section 5.1.2. The measuring setup can be seen in Figure 5.5. In this measurement the cable is short circuited in one end and the total length of the cable is 1.46 meter back and and fourth.

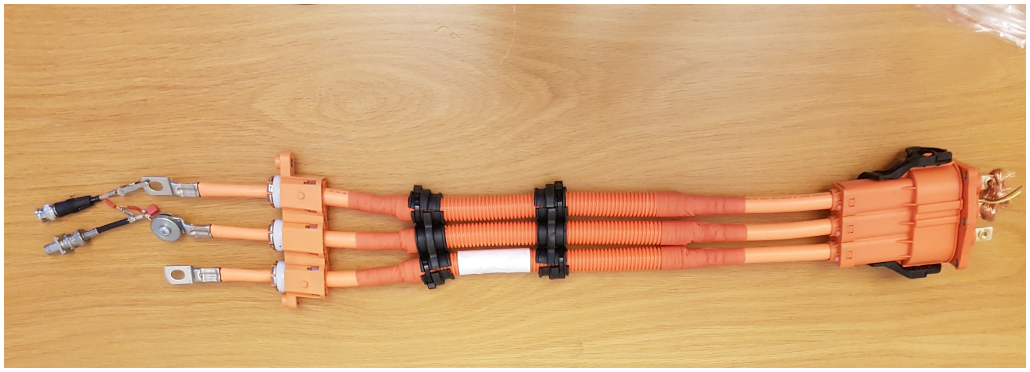

Figure 5.5: The measuring set up for the standard cable with the contactors and contact circuit.

The inductance of the cable is measured for a few different cases where the shield is connected in different ways. The ways the shield is connected is seen in the list below:

- Grounded shield: The shields of the two cables are short circuited at both ends and grounded in one end.
- SC and Free potential: The shields of the two cables are short circuited at both ends and at floating potential.
- Free potential shield: The shields of the two cables are open and at floating potential.

The results of all the measurements preformed can be seen in Figure 5.6. It can be noticed a small variation of resonant frequency depending on how the shield is connected. The reason is that the connections affect the way current flows in the shield which then affects the electromagnetic coupling between the parallel cables similar to what was observed for the long cable measurements.

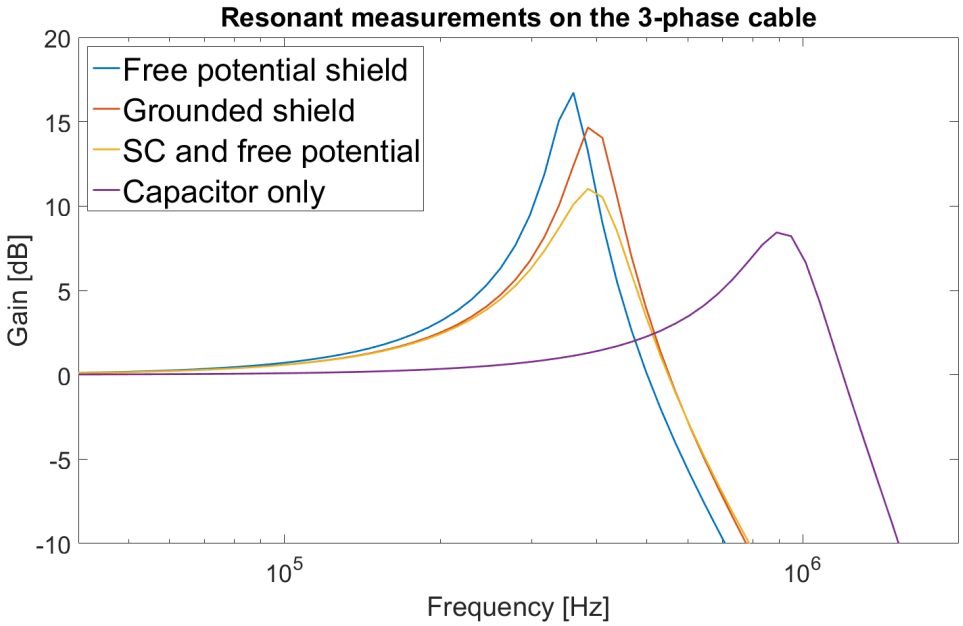

Figure 5.6: Results from the resonant measurements on the 3-phase cables.

It can be observed from Figure 5.6 that resonance occurs at 890 kHz for the contact circuit and around 380 kHz when the cable is connected. The total inductance of the measuring setup and the inductance of the contact circuit can be derived to 0.53 uH and 0.097 uH respectively, using (2.18). If the inductance of the contact circuit is subtracted from the total inductance, the inductance of the cable can be calculated to 0.43 uH or 0.295 uH/m. This seams reasonable since it is below what is measured for 7 cm separation and above whats measured for 0 cm separation for the long cable measurements.

5.2 Capacitance Measurements

To measure the capacitance between two conducting objects, the objects can be connected in series with a resistor with known resistance so that a capacitor-resistor series circuit is created. The capacitance can be found by applying a signal over the capacitor-resistor circuit and measuring the voltage at the node between the resistor and the capacitive element. The value of the capacitance can then derived from the transfer function for the voltage at the node using voltage deviation

$$V_{out} = \frac{R}{\frac{1}{jwC} + R} V_{in} \Rightarrow \frac{V_{out}}{V_{in}} = \frac{jwcR}{1 + jwcR} \tag{5.1}$$

where V_{out} is the voltage at the node, V_{in} is the voltage of the signal applied at the capacitance terminal.

To find the capacitance between the inner conductor and the shield of the standard cable the signal is applied on the inner conductor and the shield is connected to ground through a 120 Ω resistor. The voltage is then measured at the node between the shield and the resistor. The capacitance between the shields of two cables is

measured using the same method. The amplitude of the measured voltage divided by the applied voltage $\frac{V_{out}}{V_{in}}$ can be seen in Figure 5.7. In appendix A.3 the same measurements but for the cable with common shield are shown. For the inner conductor to shield measurement the length of the cable is 10.14 meter and for the measurement between the shields the cable is cut in half so that the length is 5.07 meter. The instrument used in this measurement is the Omicron Bode 100.

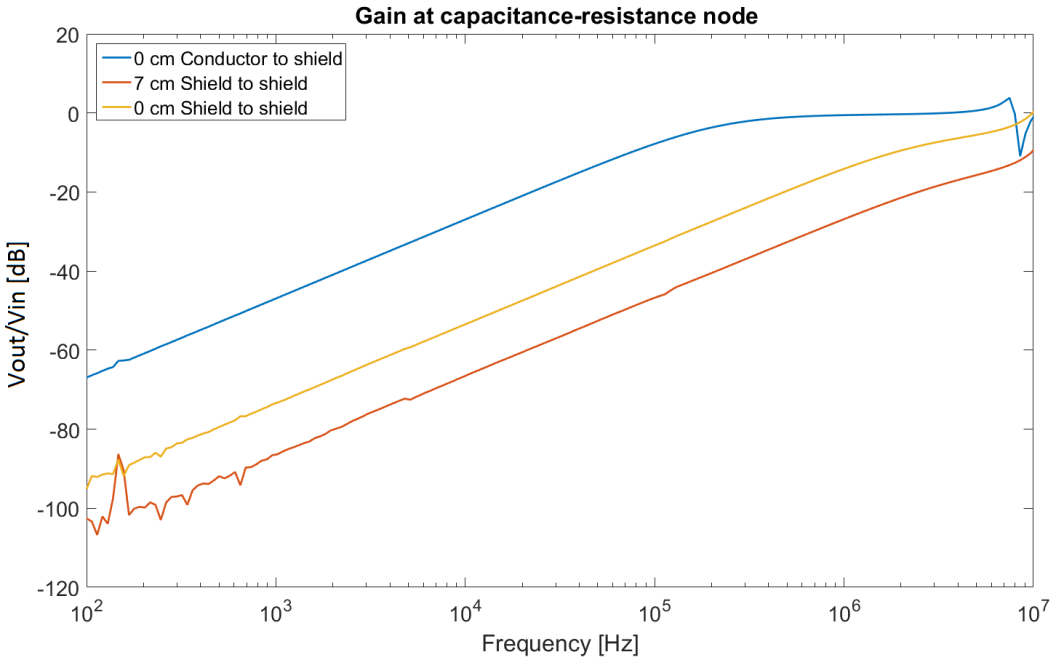

Figure 5.7: Gain at the capacitance-resistance node for a 10.14/5.07 meter long FHLR2GCB2G $35mm^2$ Coroplast cable.

By using (5.1) together with the data in Figure 5.7 it is possible to derive the capacitance-frequency graph which can be seen in Figure 5.8 for the inner capacitance and in Figure 5.9 for the outer shield to shield capacitance.

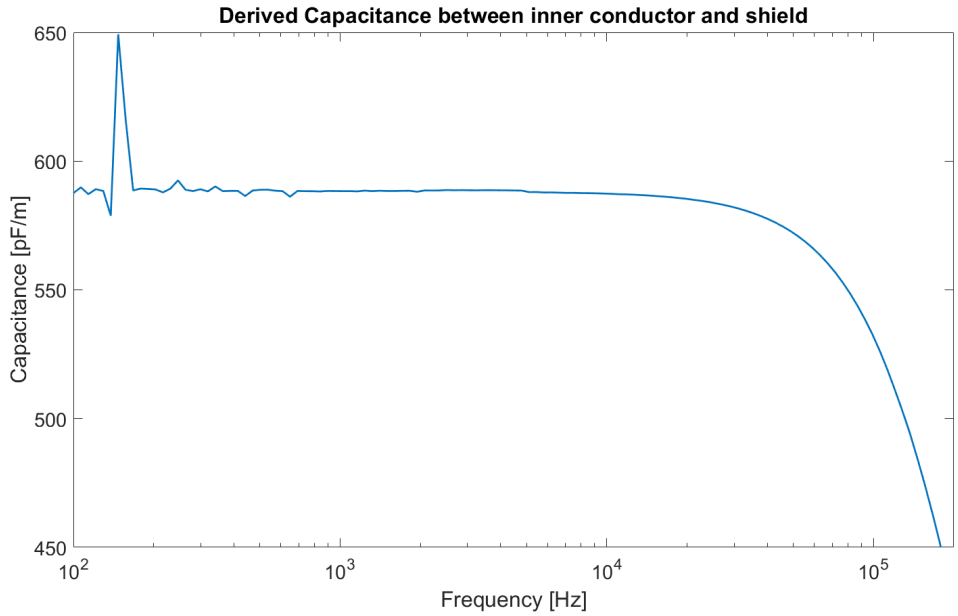

Figure 5.8: Derived inner capacitance for various frequencies.

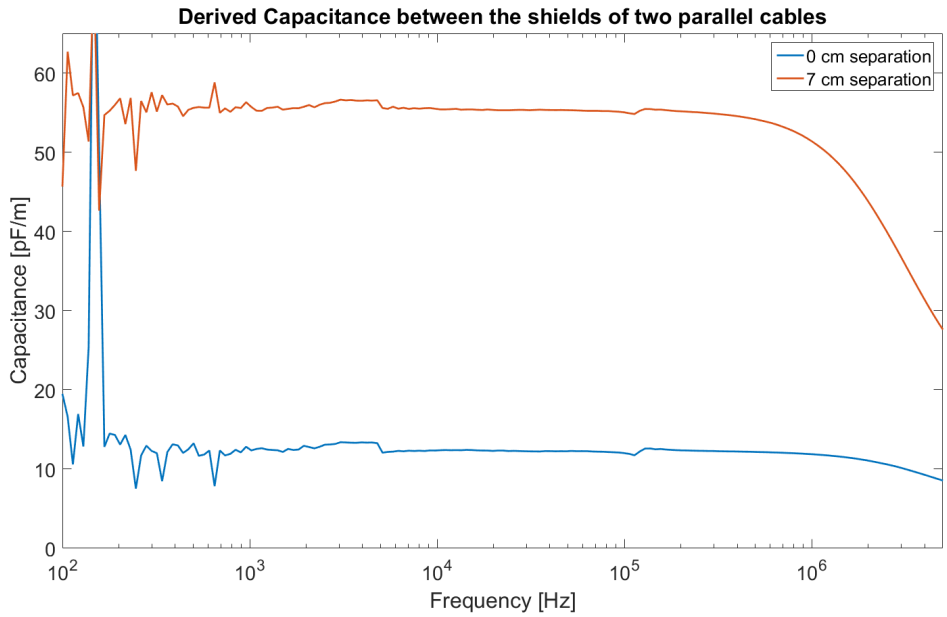

Figure 5.9: Derived outer capacitance for various frequencies.

In Figure 5.8 and 5.9 the capacitance should be constant only in the $1 >> jwcR$ region due to the way it is calculated. The high deviations at low frequencies are the result of the magnitude of signal being close to the noise floor. The derived capacitance's from all the measurements can be found in Table 5.2.

Table 5.2: Measured capacitance's for the standard cable and the common shielded cable.

Cable configuration	Inner conductor to shield [pF/m]	Shield to shield 0/7 cm[pF/m]	Conductor to Conductor [pF/m]
Single core	588	55.5 / 12.5	-
Common shield	258	-	42.2

5.3 Capacitance and Inductance Simulations

Capacitance and inductance has been derived in Chapter 3 for free copper wire geometries. In this chapter the capacitance and inductance will also be derived for the Coroplast power cables geometries.

5.3.1 The Inductance and Inductive Coupling for Different Cables

When looking at the results from the measurements it is clear that the shield plays an important role regarding the inductance of the cable. As known from (2.25) the inductance is dependant on the total magnetic flux which is reduced by a copper shield at higher frequencies as can be seen in section 4. Therefore it is interesting to determine the inductance of the cable not only for stationary but also for the higher frequency span.

To analyze this, two simulations were preformed in Comsol for 7 cm cable separation and 0 cm cable separation. A frequency domain study was used with the same geometry, material and mesh settings as in section 4. To find the inductance the total magnetic energy found from the simulation was inserted into (2.12). The results of the inductance found through simulations can be seen in Figure 5.10.

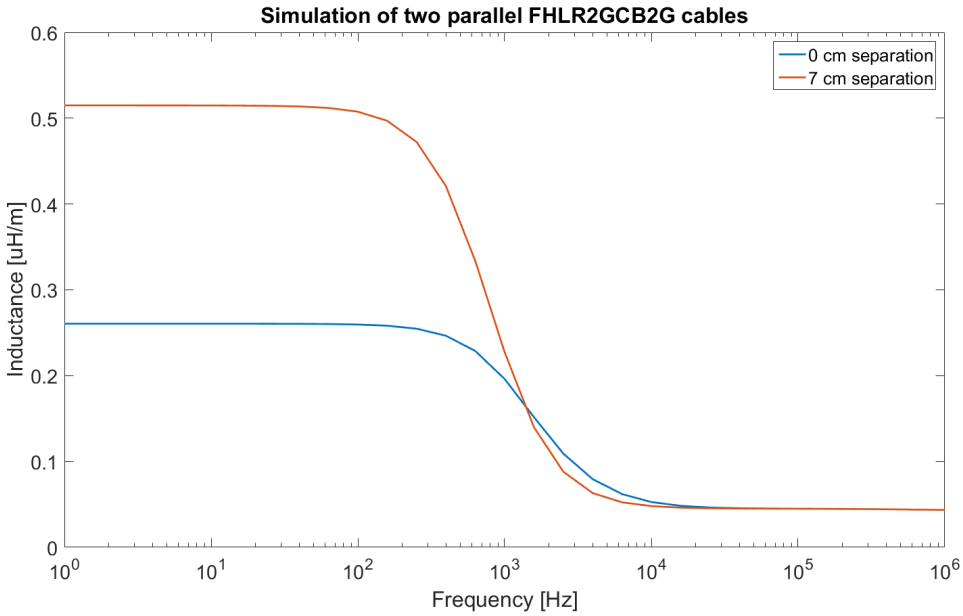

Figure 5.10: Inductance for two parallel standard shielded cables for frequencies between 1 Hz and 1 MHz.

From Figure 5.10 it can bee seen that the 7 cm and 0 cm separations curves differ significantly at low frequencies and then line up at higher frequencies. Unexpectedly does the 7 cm separation curve have a lower inductance than the 0 cm separation curve in the 2000 Hz to 10 kHz region. To analyze the inductance-frequency behaviour further it is interesting to look at the current induced in the shield. This can be derived in Comsol using surface integration of the current density on the shield domain and the results can be seen in Figure 5.11 for 0 cm separation and the 7 cm separation can be found in Appendix A.9.

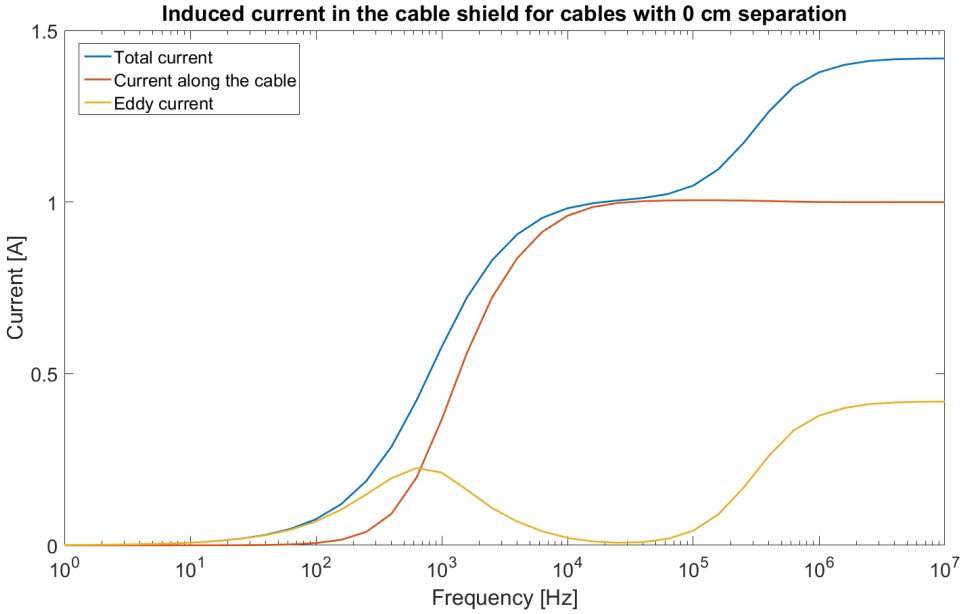

Figure 5.11: Induced currents in the shield for 0 cm cable separation for frequencies between 1 Hz and 10 MHz.

By comparing Figure 5.10 to Figure 5.11 it can be noticed that the inductance starts to fall at the same frequency as a significant amount of current is induced in the shield. A test was conducted where the shield was removed and for this case the inductance remained constant at the same level as for 1 Hz with shield regardless of the frequency. For the cable with the common shield a similar test with similar result was also conducted and the results can be found in appendix A.4.

Since the geometry of the shield used in the simulation represents a solid metal and not a meshed net of wires, the induced currents derived from simulations may differ a lot to the real cable. This will affect the induced currents significantly and the results in Figure 5.11 should be considered as a way to get a better understanding rather than an accurate simulation of the real cable.

A summary of the inductance data for the different cables at 1 Hz and 100 kHz derived from the simulations can be seen in Table 5.3. Note that the shield inductance in the table means the inductance when current is applied directly on the shield and not the inner conductor.

Table 5.3: Inductance derived from simulations for the different cables.

Cable configuration	Inductance at 1 Hz 0/7 cm [nH/m]	Inductance at 100 kHz 0/7 cm [nH/m]
Standard cable	261 / 515	45.0 / 45.0
Shield inductance	194 / 464	194 / 464
Common shield	210 / -	52.3 / -
Unshielded cable	217 / 526	217 / 526

If the inductance derived from the simulations is compared to the measured inductance shown in Table 5.1, it can be noticed that the inductance at 1 Hz from

the simulations matches the inductance measured with open shield. This is because there is almost no induced current in the shield at 1 Hz and the shield when open does not allow for current to circulate. The unshielded cable is not affected by the frequency since there is no shield where current can be induced.

A significant deviation in inductance can be noticed when comparing the inductance for the standard cable at 100 kHz from the simulations to the inductance measured with the shield grounded. The reason for this can be that the shield which have a lot of influence on the inductance for higher frequencies is meshed in reality while in the simulations it is a perfect solid metal. The induced currents will therefore experience higher resistance in the real cable shield compared what the simulated current experiences.

5.3.2 Inductance in Relation to Separation

The magnetic fields and the inductance of the cables are dependant on the distance of separation between the cables as can be seen in previous results. To find out exactly how the magnetic fields and inductance change a series of simulations were conducted for the 3-phase and DC configurations. This was done in Comsol using a paramedic sweep for a stationary study. This means that no induced currents in the screen are taken into consideration. The inductance is calculated using (2.12) and the cables are placed 60 mm above a ground plane. For AC the currents were applied with a 120° phase shift for each phase and the inductance was calculated for a periodic sweep from 0 to 2π. The inductance is then determined by the average inductance over one period i.e. the same way as for the fields.

For the 3-phase system two arrangements were tested, one with the cables in line and one with a delta cable configuration. For the configuration with the cables in line the separation distance is the total airspace between both outer cables. For the delta configuration the top cable were moved the same distance as the other cables but in a vertical path. The middle were therefore moved half the separation distance in a vertical path. The results of the simulations can be seen in Figure 5.12.

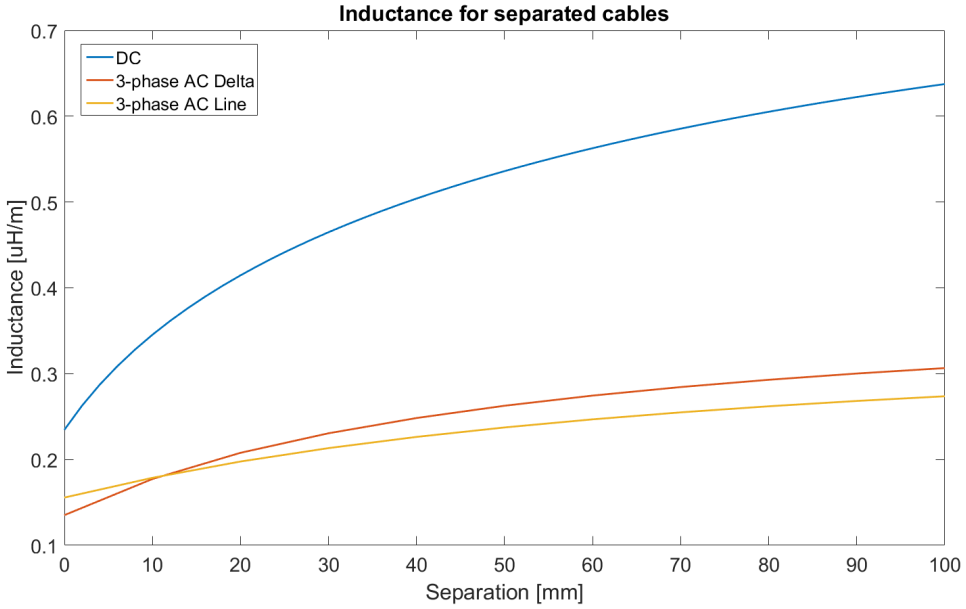

Figure 5.12: Total inductance for DC and 3-phase AC standard cable at different degree of separation.

It can be noticed that separation of the cables has a significant affect on the inductance, especially on the two DC cables. This can be explained with the return path of the current. When current in both directions follows closer to each other the field and stored energy in the air around the conductors are reduced. In the case for AC, when no current flows in the middle conductor the separating distance is the same as for DC. This is the worst case for the magnetic fields. Therefore the AC link will have lower average inductance than the DC link.

5.3.3 The Cable and Shields Capacitive Coupling

The capacitance coupling between the inner conductors to the shield and between the shields of the two cables can be determined using electrostatics and assigning voltage terminals to the shields and inner conductors. This way Comsol are able to calculate the capacitance matrix from which the capacitive coupling between the terminals can be derived. The results of the capacitance derived from the Comsol simulations are seen in Table 5.4.

Table 5.4: Capacitance for the standard cable and the common shielded cable calculated using Comsol simulations

Cable configuration	Inner conductor to shield [pF/m]	Shield to shield 0/7 cm [pF/m]	Conductor to conductor [pF/m]
Single core	1049	76.5 / 11.0	-
Common shield	739	-	63.5

The external capacitance derived from the simulations are similar to the capacitance measured which can be seen in Table 5.2. However the internal capacitance

does not match as well. This is because the minimum thickness of the insulation is used, if the capacitance is calculated analytically using (2.15) the capacitance can be calculated to 1053 pF/m, close to the value derived from simulation. It can be noticed from (2.15) that small changes for the inner conductor radius and the insulation thickness affects the capacitance significantly. Another explanation to why the results differ is that the permittivity of the insulation material used in the simulations is not the same as for the real cables.

5.4 Cable Model Evaluation

The measured cable parameters can be inserted in to the cable model used in Chapter 3. If the inductance of the cable is measured the cable model can then be compared to the measurement and evaluated. Therefore a series of differential mode impedance measurements was conducted.

The measurements were conducted using the Bode 100 and a 5.07 meter long standard shielded cable with the same setup as for the impedance measurements. The shield was either open or grounded using approximately 20 cm long cables for the connections. The result of the measurements together with the simulations can be seen in Figure 5.13 and 5.14. The resistances used in the model was calculated using (2.4). The coupling factor can be calculated to 0.785 for 0 cm cable separation and 0.916 for 7 cm cable separation using (3.1) with the measured inductance for the shielded cable from Table 5.1. The results from the simulations in Figure 5.14 is from two simulations, one where the contact between the shields are ideal and one where resistance of 0.01 Ω and inductance of 0.25 μH is added to mimic the real measurement.

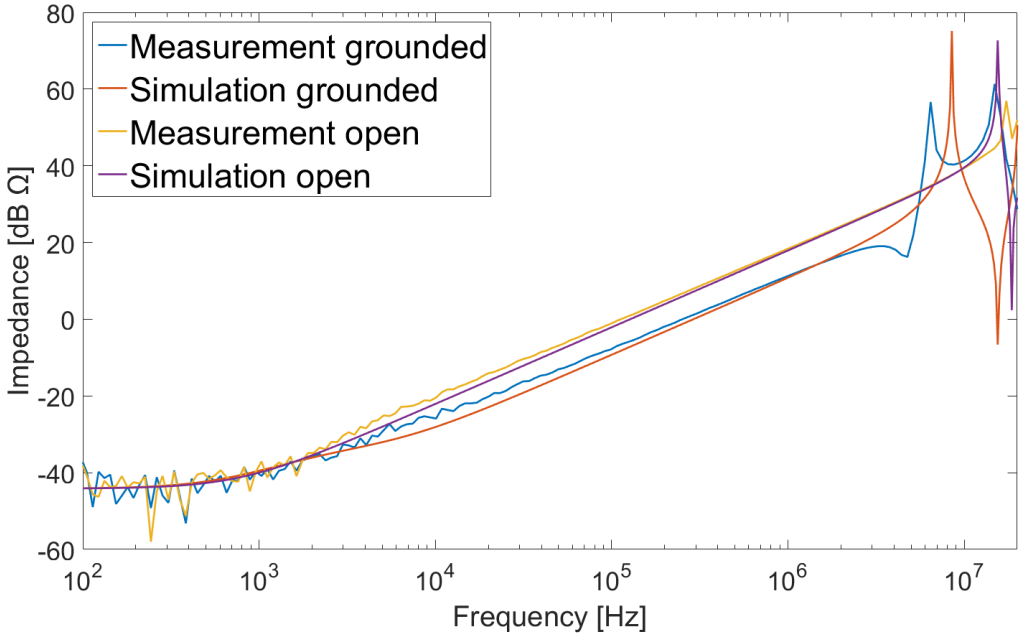

Figure 5.13: Measured and simulated differential mode impedance for the standard cable with 0 cm cable separation.

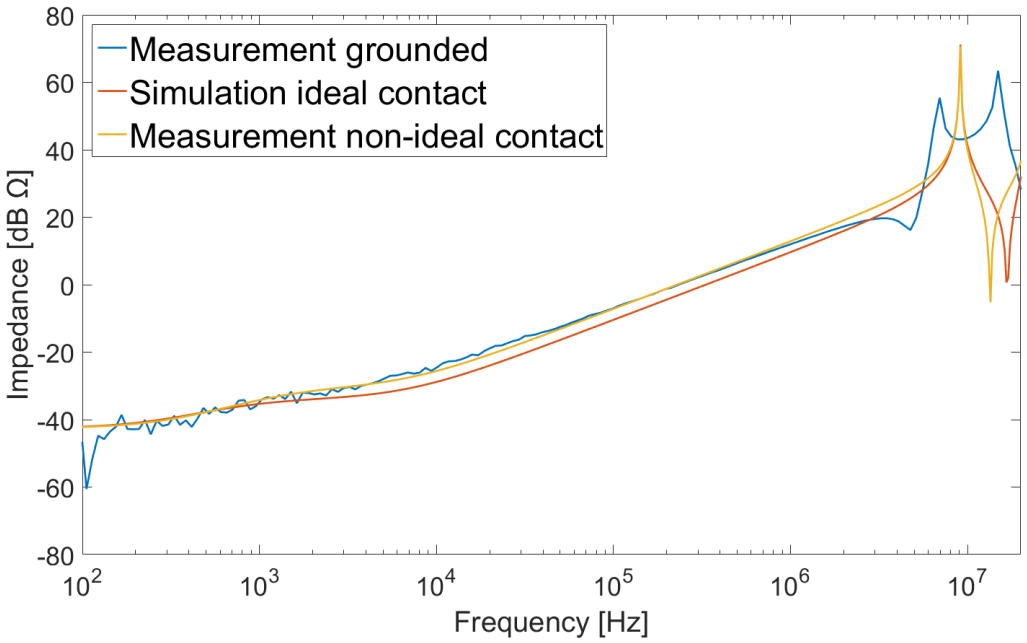

Figure 5.14: Measured and simulated differential mode impedance for the standard cable with 7 cm cable separation.

From the results it can be noticed that in the region between 100 Hz and 1 MHz there is a good match between the model and the actual measurements. Above 1 MHz the match is not as good. This is probably because the model does not take account for all capacitive couplings, such as shield to shield and shield to ground.

6

Ethical and Environmental Viewpoint

During the progress of the project a number of ethical problems had to be taken into consideration. In this chapter the most important of them will be discussed. Furthermore the topic of sustainable development regarding hybrid vehicles in general is also discussed in this chapter.

6.1 Code of Ethics

During the progression of the project a number of ethical questions had to be taken into consideration. The questions has been addressed following the IEEE Code of Ethics, where there is a number of issues that needs to be identified and handled the way the code of ethics states [32]. The most relevant issues for this project are:

Since this project focus on modeling different cables and not building a complete cable set, it can not be promised that the cable will be perfect and without flaws. If the cable design with stiffer design is used in the cars, the cable will have less mobility and therefore be harder to handle. This may lead to higher risk of mistakes and injures for the workers at the walkway in the factory where the stress is extremely high.

It is not unknown that almost every company wants to save money when building or developing some sort of project or product. Therefore it is very important to resist any kind of bribery, for example paying "us" so the design of the cables will be cheaper but the electromagnetic radiation is greater then what is allowed and therefore may be causing injures from electromagnetic exposure as mentioned in 1.3.3. Also signal cables could be induced with current and wrong signals could be delivered and cause in worst case a major fault in the car.

The project was partly done at RISE and some test with high voltage was done therefore it was extremely important to be careful to not harm or injure anyone, also it was important to be careful to not destroy the expensive equipment that was to the groups disposal such as a network analyzer.

According to IEEE code of ethics, "to seek, accept, and offer honest criticism of technical work, to acknowledge and correct errors, and to credit properly the contributions of others". For most this is common knowledge, when the presentation of the project and the opposition was done the group was very pleased and thankful with the comments and took it in to consider.

6.2 Development for a Sustainable Future

To give the future generations the same opportunity to meet their needs as we have it is important to have the sustainable aspect in mind. When developing new products the term sustainable development is often used. Sustainable development can be very broad and unclear, but the definition used in this report is the definition G.H. Brundtland introduced:

> "Sustainable development is development that meets the needs of the present without compromising the ability of future generations to meet their own needs"
>
> -G.H. Brundtland, Our Common Future, 1987.

For electric and hybrid cars sustainable development can be dived in to three parts, ecological, economical and social.

The point of electric drive in electric and plug-in hybrid vehicles is to reduce the emissions. When the energy produced by fossil fuels are used in the electric driven cars there is no point in it, the emissions will only be reduced if the electric energy comes from renewable energy source such as water or wind power, or nuclear energy source. However another perspective of this can be if more electric and hybrid vehicles is being used then the need of more clean energy is therefore also needed which forces us even more to use clean energy. Also the potential of reducing the total global emissions by the use of clean electrical power sources is larger as it can effect the transport sector.

One of the drawbacks with the use of renewable sources is that it can affect the ecological system. An example of this is for wind power where if more wind mills where build and used, more animals could get hurt or even killed, such as bats by flying into the spinning blades [33].

Electric and hybrid vehicles are great for environment when it comes to emission compared to the standard combustion engine car, however it comes with an economical expense. Since a hybrid car have two engines it is more expensive and both hybrid and pure electric have lots of batteries and the cost is most often higher than for a standard ICE car.

More electric propelled vehicles are made and therefore more materials for the electric machine is needed, some of them are rather rare such as Neodymium Iron Boron (NdFeB). Since this is rare and therefore not very cheap, the price with a large risk will rise with time and not be very economical. Some sort of replacement material needs to be used or the electric motor needs to be switched to a cheaper but with less performance for it to be sustainable [34].

When driving pure electric which is the best for the environment the car has a limited range. Therefore driving from work and home these cars are great since it can recharge when standing still, but for long distance travel and vacation traveling the fail cause of the limiting range and long charging time compared to the ICE car. These together with the economical perspective are the main points which

unfortunate makes these vehicles less attractive [35].

Since people are concerned about the environment and hybrid and electric cars are expensive. This can be a big incentive for people to purchase electric and hybrid cars in societies where they are considered as status symbols. This way the social factor can drive the sustainable development further.

7
Conclusion

According to measurements conducted on the test rig the main current ripple noise occurs in the frequency range of 10 kHz to 100 kHz. To reduce the magnetic fields caused by the current a shield around the cable can be used. The simulations and measurements shows that shielding with a copper material greatly reduce the electromagnetic fields around the cables in the higher frequency range as long as it is properly connected. To reduce the magnetic field at lower frequencies magnetic materials with high permeability such as mumetal must be used. Combining both copper and mumetal will increase the shielding effectiveness even further at low frequencies. This since the mumetal will increase the magnetic coupling so that a significant amount of current is inducted in the copper even at low frequencies.

Another way to mitigate the magnetic field is to change the cable arrangement and/or its geometry. Depending on what interfering frequencies occurs, different setups can be applied such as use two conductors on each phase, using a common shield or twisting the cable. A general rule is that the closer the conductor are to each other the better field cancellation effect it gets.

When it comes to determining the parameters of the cable, the resonant measurements conducted shows that the inductance of the shielded cable is dependant on the way the shield is connected. The reason for this is that current needs to be able to flow in the shield along the cable in order to affect and reduce the inductance. When the shield is connected the measured inductance is very similar to the given inductance in the data sheet for the cable where as the same goes for the measured capacitance. However when it comes to the simulations, the derived parameters are not as similar.

The cable model which takes the shield in consideration and thus the changing inductance was tested by comparing it to the real cable. The results indicates that the model works properly in the 100 Hz to 1 MHz region if the connection resistance and inductance are included in the model. However at higher frequency the accuracy of the model is reduced.

Bibliography

[1] ICNIRP, "Icnirp guidelines for limiting exposure to time-varying electric and magnetic fields (1hz - 100 khz)," *Health Physics*, vol. 99, 2010. [Accessed 17 Jan, 2017].

[2] Matweb Material Property Data, "Momentive performance materials rtv31 silicone rubber compound for high temperature, red."

[3] International Council on Clean Transportation, "Programs / passenger vehicles."

[4] "Regulation (ec) no 443/2009 of the european parliament and of the council of 23 april 2009." `http://eur-lex.europa.eu/legal-content/EN/TXT/PDF/?uri=CELEX:02009R0443-20140408&from=EN`. [Accessed 17 Jan, 2017].

[5] International Council on Clean Transportation, "China phase 4 passenger car fuel consumption standard proposal," *INTERNATIONAL COUNCIL ON CLEAN TRANSPORTATION*, mar 2014.

[6] Delphi, "Worldwide emissions standards," 2016.

[7] Schaffner, "Basics in emc / emi and power quality," Nordstrasse 11 4542 Luterbach Switzerland, 2013.

[8] G.L. Skibinski, R.J. Kerkman, D. Schlegel, "Emi emissions of modern pwm ac drives," *IEEE Industry Applications Magazine*, vol. 5, pp. 47–80, nov 1999.

[9] Nobuyoshi Mutoh, Senior Member, IEEE, Mikiharu Nakanishi, Masaki Kanesaki, and Joji Nakashima, "Emi noise control methods suitable for electric vehicle drive systems," *TRANSACTIONS ON ELECTROMAGNETIC COMPATIBILITY*, vol. 47, pp. 930–937, nov 2005.

[10] Dudi A. Rendusara, Student Member, IEEE, and Prasad N. Enjeti, Senior Member, IEEE, "An improved inverter output filter configuration reduces common and differential modes at the motor terminals in pwm drive systems," *TRANSACTIONS ON POWER ELECTRONICS*, vol. 13, pp. 1135–1143, nov 1998.

[11] Hirofumi Akagi, Fellow, IEEE, and Takafumi Doumoto, "An approach to eliminating high-frequency shaft voltage and ground leakage current from an inverter-driven motor," *TRANSACTIONS ON INDUSTRY APPLICATIONS*, vol. 40, pp. 1162–1169, jul 2004.

[12] World Health Organization, "Environmental health criteria 238 extremely low frequency fields," *the International Labour Organization, the International Commission on Non-Ionizing Radiation Protection, and the World Health Organization*, 2007. [Accessed 17 Jan, 2017].

[13] William H. Hayt, Jr. Jhon A. Buck, *Engineering Electromagnetics*. McGraw-Hill, eighth ed., 2012.

[14] Daniel Fleisch, *A Student's Guide to Maxwell's Equations*. Cambridge University Press - M.U.A, jan 2008.
[15] Cao Wei, R.F. Harrington, J.R. Mautz, T.K. Sarkar, "Multiconductor transmission lines in multilayered dielectric media," *IEEE Transactions on Microwave Theory and Techniques*, vol. 32, pp. 439 – 450, 1984.
[16] D. P. Kothari,I. J. Nagrath, *Modern Power System Analysis*. Tata McGraw-Hill, third ed., 2003.
[17] N. Mohan, T. Undeland and W. Robbins, *Power Electronics*. Jhon Wiley & Sons Inc., second ed., 1995. Page. 254.
[18] Alastair R. Ruddle, Lester Low, Rob Armstrong, Linda Dawson and Andrew Rowell, "Recommendations for mitigating low frequency magnetic field exposure in hybrid/electric vehicles," tech. rep., MIRA Limited, York EMC Services Limited, 2014.
[19] Per Pettersson, Niclas Schonborg, "Reduction of power system magnetic field by configuration twist," *IEEE Transactions on Power Delivery*, vol. 12, no. 4, 1997.
[20] Salvatore Celozzi; Rodolfo Araneo; Giampiero Lovat, *Electromagnetic Shielding*. Wiley-IEEE Press, 2008.
[21] A.S. Farag , M.M. Dawoud, I.O. Habiballah, "Implementation of shielding principles for magnetic field management of power cables," *Electric Power Systems Research*, 1999.
[22] Surendra Loya, Habibullakhan, "Analysis of shielding effectiveness in the electric field and magnetic field and plane wave for infinite sheet metals," *International Journal of Electromagnetics and Applications*, 2016.
[23] Cindy S. Cheung, "Shielding effectiveness of superalloy, aluminum, and mumetal shielding tapes," tech. rep., California Polytechnic State University at San Luis Obispo, 2009.
[24] Analog devices, "Emi, rfi, and shielding concepts, tutorial mt-095," 2009.
[25] Mushield company inc, *Mushield- Catalog and Design guide*.
[26] Masud Mansuripur, Armis R. Zakharian, "Maxwell's macroscopic equations, the energy-momentum postulates, and the lorentz law of force," *PHYSICAL REVIEW*, nov 2009.
[27] Magnetic field and HF cable modeling and validation: M1 Peter Ankarson, Urban Lundgren, Jan Carlsson, "Magnetic field and hf cable modeling and validation: M1," tech. rep., SP Technical Research Institute of Sweden, 2016.
[28] Azo Materials, "Silicone rubber," sep 2001.
[29] J. F. Dexter and P. C. Servais, "Silicone rubber as cable insulation," tech. rep., Dow Corning Corporation Midland, Michigan, 1967.
[30] Coroplast Fritz Müller GmbH & Co. KG, *Shielded cable for automotive electric powertrain, Coroplast Part No.: 9-2611 / 35 mm2*.
[31] Mushield company inc, "Mumetal specifications."
[32] IEEE, "Ieee code of ethics." `http://www.ieee.org/about/corporate/governance/p7-8.html`, November 2016. [Accessed 24 Nov, 2016].
[33] Kunz, Thomas H. and Arnett, Edward B. and Erickson, Wallace P. and Hoar, Alexander R. and Johnson, Gregory D. and Larkin, Ronald P. and Strickland, M Dale and Thresher, Robert W. and Tuttle, Merlin D., "Ecological impacts of

wind energy development on bats: questions, research needs, and hypotheses," *Frontiers in Ecology and the Environment*, vol. 5, no. 6, pp. 315–324, 2007.

[34] James D. Widmer, Richard Martin, Mohammed Kimiabeigi, "Electric vehicle traction motors without rare earth magnets," *Sustainable Materials and Technologies*, 2015.

[35] Christian Hanke, Michael Hülsmann and Dirk Fornahl, "Socio-economic aspects of electric vehicles: A literature review." University Bremen.

A

Appendix 1

A.1 Crosstalk Copper wires above Ground Plane

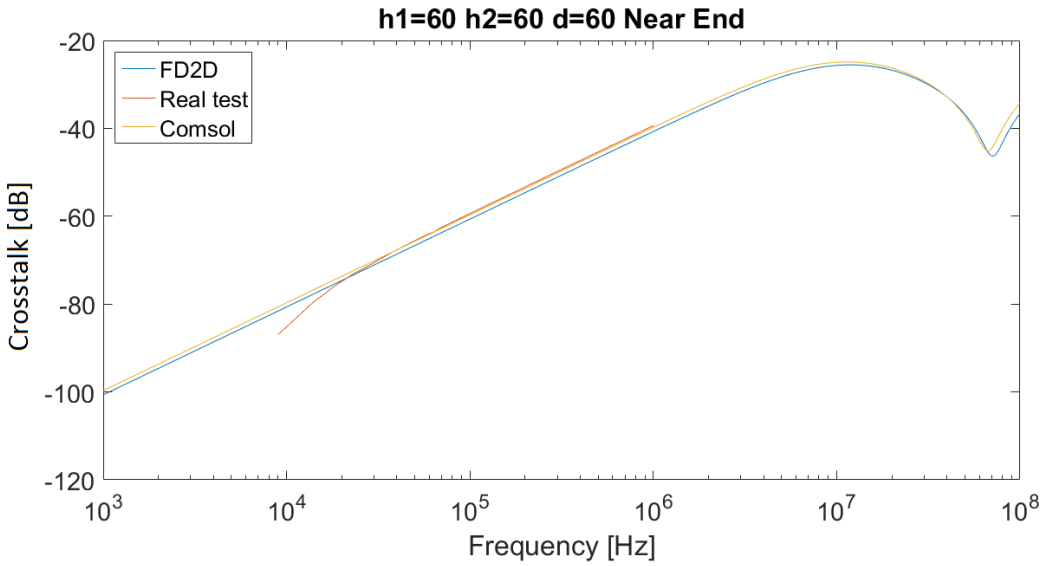

Figure A.1: Crosstalk between two wires 60 mm above ground and 60 mm between each other.

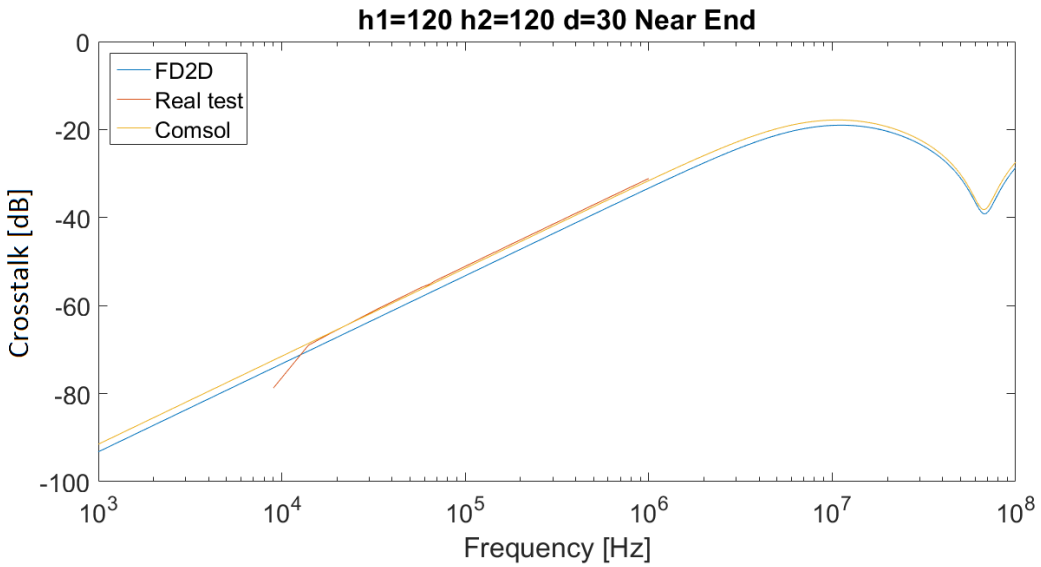

Figure A.2: Crosstalk between two wires 120 mm above ground and 30 mm between each other.

A.2 Resonant Measurements

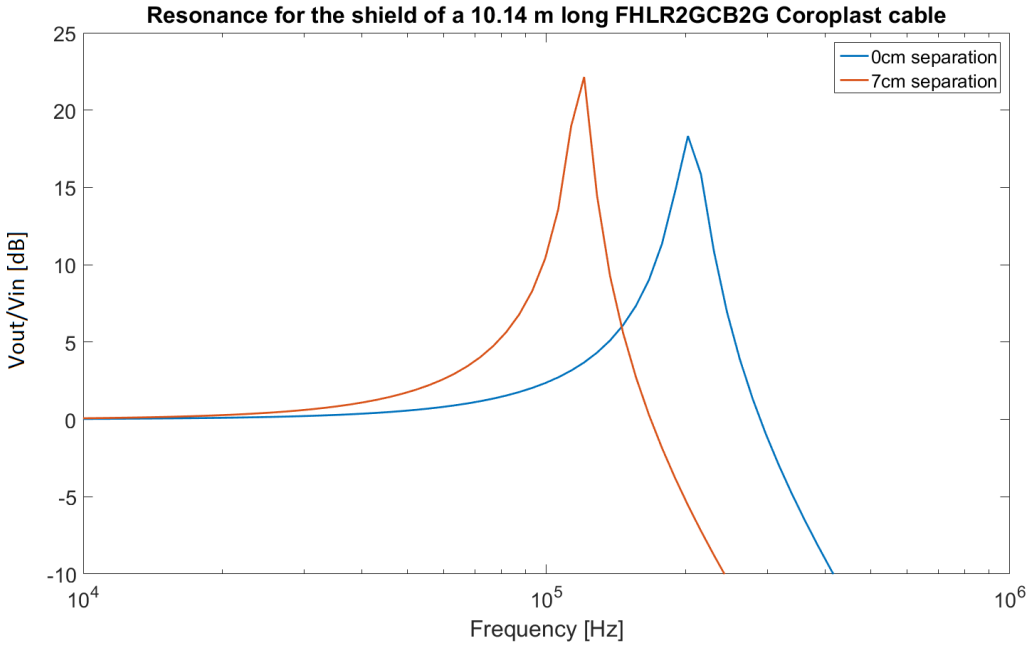

Figure A.3: Resonant frequency measurement for the shield of a 10.14 meter long FHLR2GCB2G $35mm^2$ Coroplast cable.

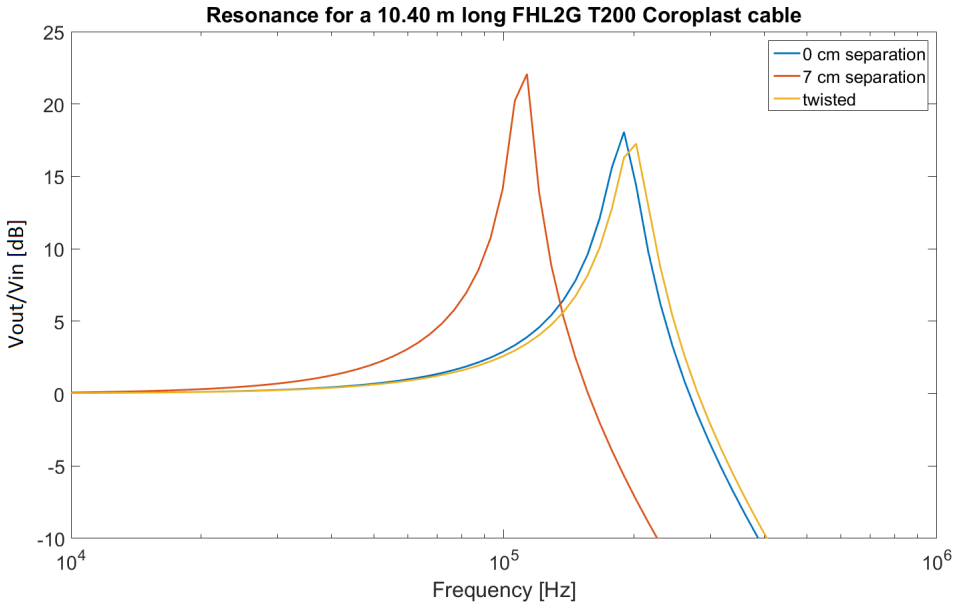

Figure A.4: Resonant frequency measurement for a 10.40 meter long FHL2G T200 $35mm^2$ Coroplast cable.

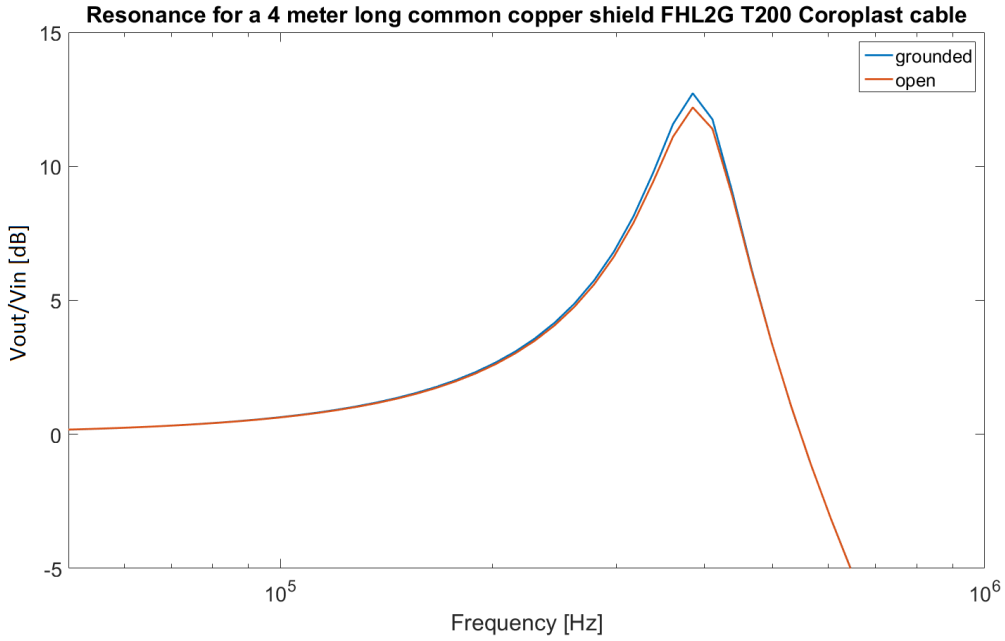

Figure A.5: Resonant frequency measurement for a common shielded 10.40 meter long FHL2G T200 $35mm^2$ Coroplast cable.

A.3 Capacitance Measurements

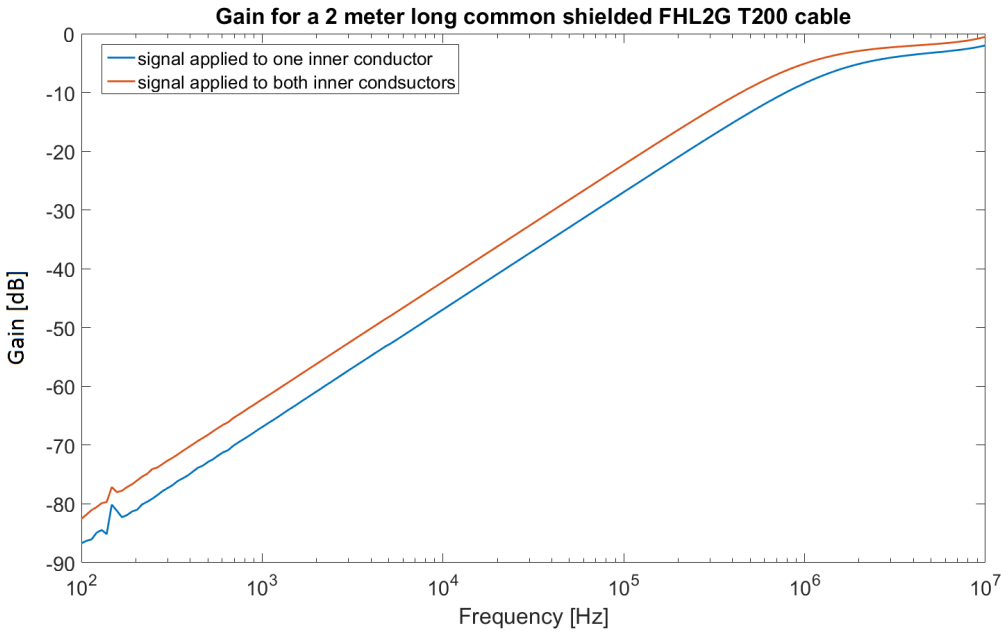

Figure A.6: Capacitance at capacitance-resistance node for a 2 meter long FHL2G T200 cable with a common shield.

A.4 Inductance Simulations

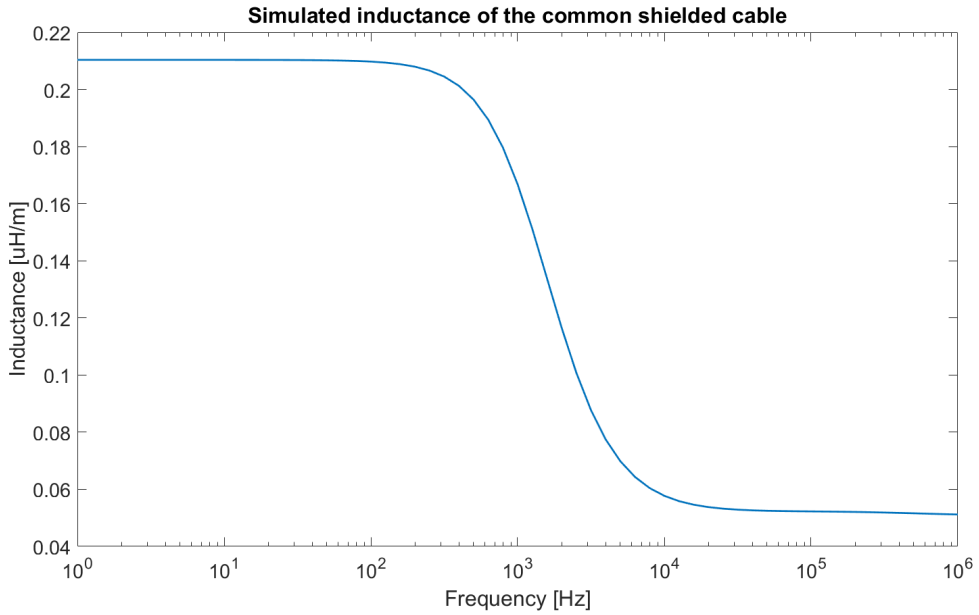

Figure A.7: Simulated inductance for the common shielded cable.

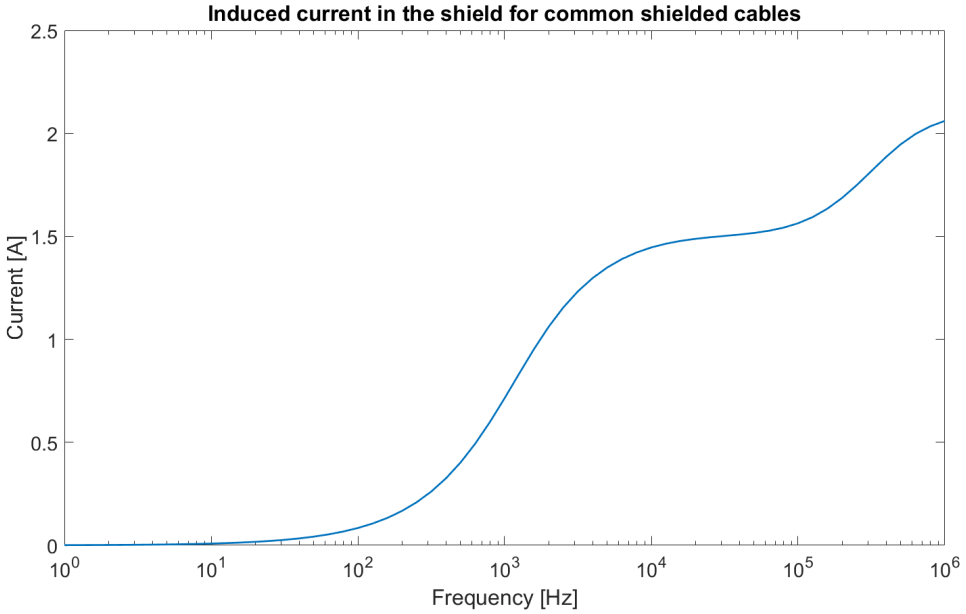

Figure A.8: Simulated induced current for the common shielded cable.

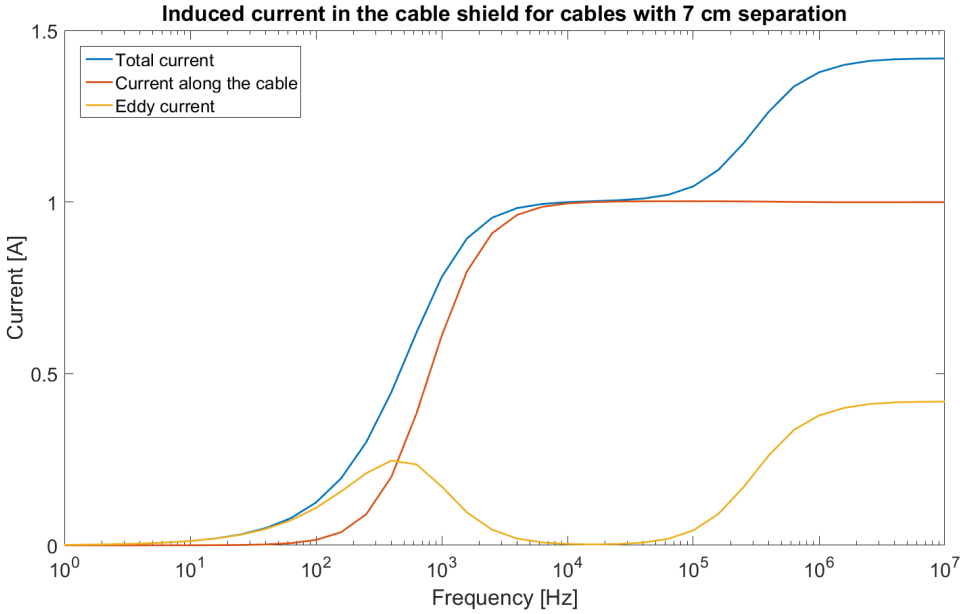

Figure A.9: Induced currents in the shield for 7 cm cable separation.

A.5 Permeability of mumetal frequency dependent

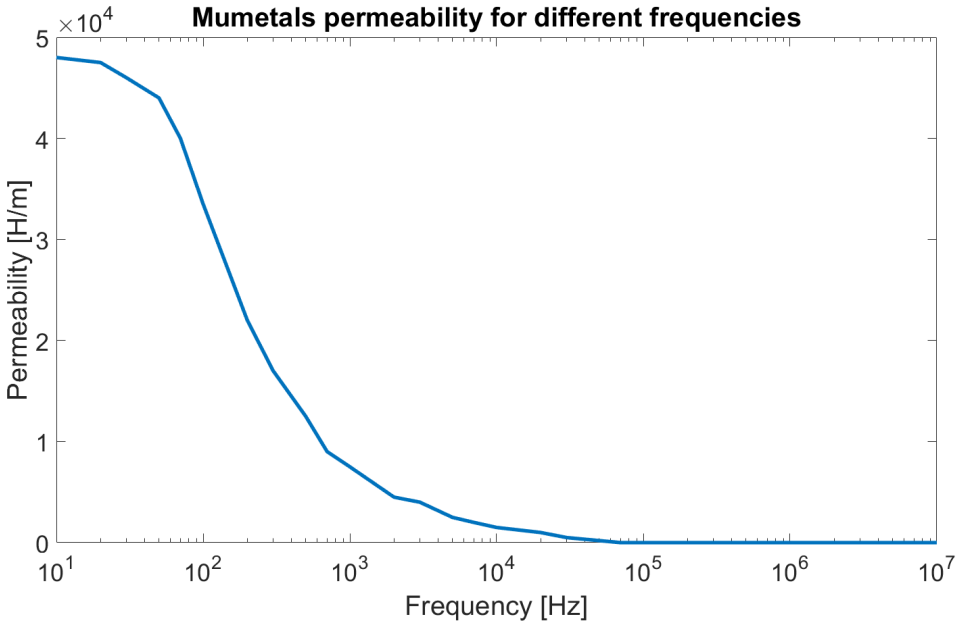

Figure A.10: Model for the mumetal material and its frequency dependent permeability property.